

# CORNELL UNIVERSITY LIBRARY

Subscriber access provided by CORNELL UNIVERSITY LIBRARY

# Characterization, Synthesis, and Modifications

# An azido-functionalized polyurethane designed for making tunable elastomers by click chemistry

Xiaochu Ding, Jin Gao, abhinav acharya, Yen-Lin Wu, Steven R. Little, and Yadong Wang

ACS Biomater. Sci. Eng., Just Accepted Manuscript • DOI: 10.1021/acsbiomaterials.9b01357 • Publication Date (Web): 31 Dec 2019

Downloaded from pubs.acs.org on January 6, 2020

# **Just Accepted**

"Just Accepted" manuscripts have been peer-reviewed and accepted for publication. They are posted online prior to technical editing, formatting for publication and author proofing. The American Chemical Society provides "Just Accepted" as a service to the research community to expedite the dissemination of scientific material as soon as possible after acceptance. "Just Accepted" manuscripts appear in full in PDF format accompanied by an HTML abstract. "Just Accepted" manuscripts have been fully peer reviewed, but should not be considered the official version of record. They are citable by the Digital Object Identifier (DOI®). "Just Accepted" is an optional service offered to authors. Therefore, the "Just Accepted" Web site may not include all articles that will be published in the journal. After a manuscript is technically edited and formatted, it will be removed from the "Just Accepted" Web site and published as an ASAP article. Note that technical editing may introduce minor changes to the manuscript text and/or graphics which could affect content, and all legal disclaimers and ethical guidelines that apply to the journal pertain. ACS cannot be held responsible for errors or consequences arising from the use of information contained in these "Just Accepted" manuscripts.

# An azido-functionalized polyurethane designed for making tunable elastomers by click chemistry

Xiaochu Dinga, Jin Gaob, Abhinav P. Acharyac, Yen-Lin Wua, Steven R. Littled and Yadong Wang\*a

- a. Nancy E. and Peter C. Meining School of Biomedical Engineering, Cornell University, 277 Kimball Hall, Hollister Drive 134, Ithaca, NY 14853.
- b. School of Dental Medicine, University of Pittsburgh, 335 Sutherland Drive, 522 Salk Pavilion, Pittsburgh, PA 15260.
- c. Department of Chemical Engineering, Arizona State University, 501 E. Tyler Mall, Tempe, AZ 85287.
- d. Department of Chemical and Petroleum Engineering, University of Pittsburgh, 940 Benedum Hall, 3700 O'Hara Street, Pittsburgh, PA 15261.

\*Corresponding author: <a href="www.yw839@cornell.edu">yw839@cornell.edu</a>

#### Abstract

Polyurethane is an important biomaterial with wide applications in biomedical engineering. Here, we report a new method to make an azido-functionalized polyurethane pre-polymer with no need of post modification. This pre-polymer can easily form stable porous elastomers through click chemistry for crosslinking, instead of using a toxic polyisocyanate. The mechanical properties can be modulated by simply adjusting either the pre-polymer concentrations or azido/alkyne ratios for crosslinking. The Young's modulus therefore varies from 0.52 to 2.02 MPa for the porous elastomers. When the APU elastomer is made with a compact structure, the Young's modulus increases up to 28.8 MPa at 0-15% strain. The strain at break reaches 150% that is comparable to the commercially resourced Nylon-12. Both the porous and compact elastomers could undergo reversible elastic deformations for at least 200 and 1000 cycles respectively within 20% strain without failure. The material showed a considerable stability against erosion in a basic solution. *In vivo* biocompatibility study demonstrated no degradation by subcutaneous implantation in mice

over two months. The implant induced only a mild inflammatory response and fibrotic capsule.

This material might be useful to make elastomeric components of biomedical devices.

# **Keywords:**

Polyurethane, elastomers, azido functionality, click chemistry, scaffolds

## Introduction

Polyurethanes (PUs) have been widely used to engineer medical devices, tissue scaffolds and prostheses.<sup>1-4</sup> It has been reported that some commonly used PU medical devices or products contained low but measurable concentrations of residual isocyanates, which caused safety concerns.<sup>5-7</sup> Scientists have been seeking new methods to make PUs for a safer use, particularly in biomedical fields. In some circumstances, PUs with reactive functional groups are highly desirable to impart functionalities for different engineering designs.8-12 For example, immobilizing anti-inflammatory or cell attachment moieties on a tissue scaffold would improve the tissue compatibility or promote cell adhesion and proliferation in the scaffolds. 13-15 Typically, a diol monomer with a protected amino or hydroxyl group is reacted with a diisocyanate, followed by de-protection to yield a PU with amino or hydroxyl groups for further functionalization. 16-19 Compared with amino and hydroxyl groups, azido functionality can more efficiently and specifically undergo click reaction with alkyne-bearing molecules under a mild condition. 18 The azide-alkyne click chemistry has been well established for biomedical applications.<sup>20</sup> Here, we report a new azido-containing diol monomer and use to make an azido-functionalized polyurethane (APU) pre-polymer. We subsequently use this pre-polymer to make a series of APU elastomers through click chemistry for studies.

Previously, the pendent azido functionality can be introduced into a PU or a polymer by post-modification of amino-, hydroxyl-, chloride-, or bromo- groups on the backbone, followed by purification.<sup>8, 11, 18, 21-23</sup> For example, a three-step method was reported to make an azido-functionalized PU. A polyether diol segment was first synthesized to bear chloride groups. This chloride-bearing polyether diol was then reacted with sodium azide and purified to obtain an

azido-containing polyether diol. Finally, this diol segment was copolymerized with butane-1,4-diol and diisocyanate to yield the resultant azido-functionalized PU.8 Alternatively, a PU was synthesized and de-protected to bear free hydroxyl groups, followed by coupling with 4azidobenzoic acid through DCC/DMAP coupling reaction and purification to introduce azido groups to the PU.18 Such post-modification and purification complicates the synthesis and also likely hydrolyzes the polymer backbone. On the other hand, a 2.2-bis-(azidomethyl)propane-1.3diol was ever synthesized to make azido-functionalized polyesters, polycarbonates and poly(ester-carbonates).<sup>24-27</sup> In this monomer, the two azidomethyl groups are attached to the same second carbon of the propane-1,3-diol, showing a limited space between the two azido groups. No literatures have reported using this bisazido diol monomer to introduce azido functional groups to PUs for utilities. Therefore, we designed a new bisazido diol monomer, 2,2'bis(azidomethyl)-triethylene glycol, to conveniently impart azido- functionality to the PUs. This bisazido diol monomer together with a polyester or polyether diol segment are reacted with a diisocyanate to yield an APU pre-polymer. The diol segment can be used to manipulate the physico-chemical and biological properties such as the mechanical properties, hydrophilicity, biocompatibility and biodegradability.<sup>1, 28-29</sup> At the proof-of-concept stage, we examined the polymerization using the designed bisazido diol and tetraethylene glycol with hexamethylene diisocyanate to make the APU pre-polymer. This pre-polymer is then crosslinked with a di-alkyne crosslinker to examine the click reactions to yield the APU elastomers. The tetraethylene glycol is selected as the ether diol segment because it is hydrophilic and biologically stable with a low glass transition temperature. These features will make the designed APU elastomers relatively stable and ease the mobility of polymer chains for reversible mechanical deformations in a biological setting.

This work focuses on the material synthesis and characterizations. FTIR, proton NMR, HPLC and GPC analyses are used to characterize the chemical structure, composition and molecular weight. Uniaxial tensile and cyclic tensile tests are performed to evaluate the

mechanical properties and the performance for reversible elastic deformations. The as-made APU elastomer is implanted subcutaneously in mice to examine the host responses.

# **Result and Discussion**

# 1. Syntheses of the bisazido diol monomer and di-alkyne crosslinker

To impart azido functionality to PUs, we designed a bisazido diol monomer for the utility. The bisazido diol is synthesized by a ring opening reaction of ethylene glycol diglycidyl ether (EGDE) with excessive sodium azide in the presence of Oxone® monopersulfate catalyst (**Fig. 1A**). This reaction could regioselectively open the epoxides in EGDE by azide anions,<sup>30</sup> which mainly yields a viscous 2,2'-bis(azidomethyl) triethylene glycol (BAG). The raw BAG is purified by flash chromatography with a purity above 97% as verified by HPLC analysis (**Fig. 1B**). The overall yield of the BAG can reach approximately 65% after purification.

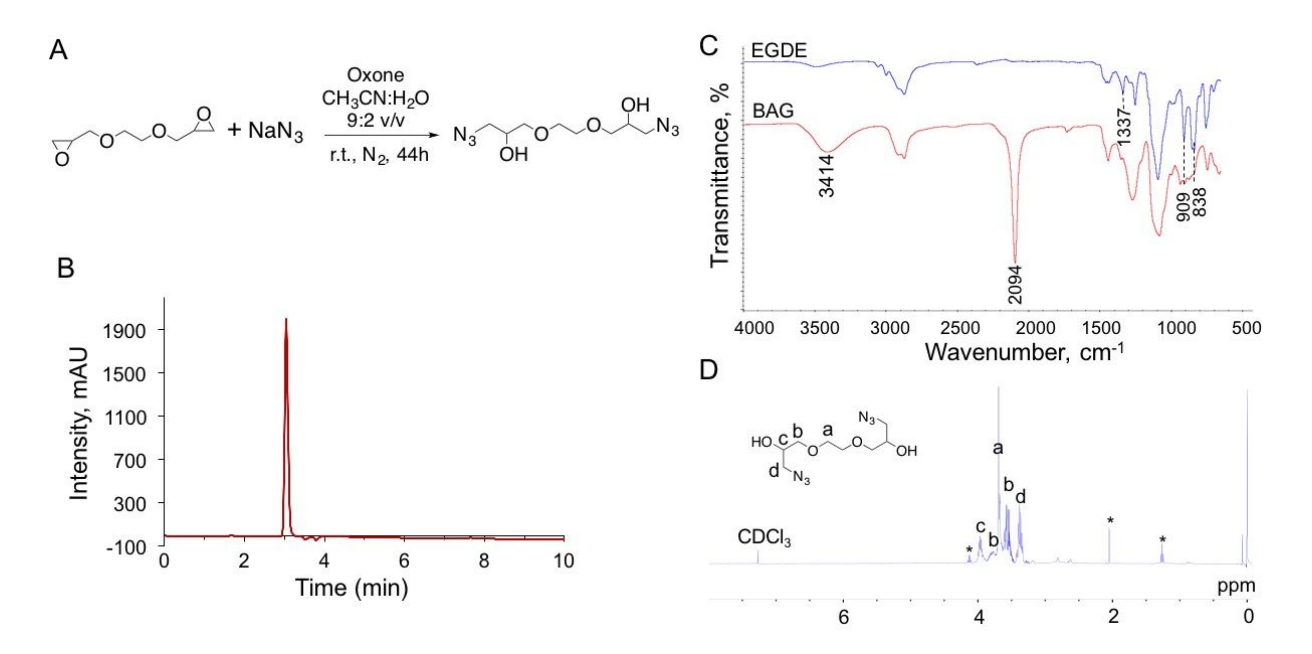


**Figure 1**. (A) Synthesis of the BAG monomer by ring opening reaction of EGDE with excessive sodium azide in the presence of Oxone® monopersulfate catalyst. The molar ratio of EGDE to sodium azide to Oxone® monopersulfate is 1 : 4 : 1. (B) HPLC analysis indicates the purity of the BAG monomer above 97% by flash chromatography. (C) Comparison of FTIR spectra of the starting EGDE and the resultant BAG monomer. The new absorptions at 3414 and 2094 cm<sup>-1</sup> are

attributed to hydroxyl and azido groups in the BAG monomer, indicating a successful azidolysis of the epoxide rings. (D) Proton NMR analysis further confirmed the chemical structure of the BAG monomer. The integral area ratio of H<sub>d</sub> to H<sub>c</sub> approaches to 2 : 1, matching well with the chemical structure of the BAG monomer (**Fig. S1**). '\*' marked chemical shifts are from the solvent residue of ethyl acetate.

FTIR and proton NMR spectroscopic analyses are used to identify the chemical structure of the purified BAG monomer (**Fig. 1C** and **D**). The FTIR absorptions of the starting EGDE at 1337, 909 and 838 cm<sup>-1</sup> disappear after the epoxide rings are opened by the azide anions. Two new absorptions are shown at 3414 and 2094 cm<sup>-1</sup>, which are attributed to the hydroxyl and azido groups in the resultant BAG monomer, indicating a successful ring opening reaction (**Fig. 1C**). Further, the proton NMR analysis confirmed the correct chemical structure of the BAG monomer. The corresponding chemical shifts ( $\delta$ s) are labeled in **Fig. 1D**. The  $\delta$ s at 3.38 and 3.97 ppm are attributed to the protons of H<sub>d</sub> and H<sub>c</sub> after the ring opening reaction of the epoxides with the azide anions. The integral area ratio of H<sub>d</sub> to H<sub>c</sub> is determined to be approximately 2 : 1 (**Fig. S1**), matching well with the chemical structure of the BAG monomer. The NMR together with the FTIR analyses well confirmed an efficient regioselective ring opening reaction between the EGDE and azide anions catalyzed by the Oxone® monopersulfate. Such regioselective ring opening reaction is consistent with a prior report.<sup>30</sup>

We further synthesized a di-alkyne (DA) as a crosslinker. The DA molecule is made from 5-hexyn-1-ol and hexamethylene diisocyanate (HDI) (**Fig. 2A**). The as-prepared DA compound could be purified by repetitive solvation in tetrahydrofuran and precipitation in diethyl ether. HPLC analysis demonstrates a purity above 96 % of the resultant DA (**Fig. 2B**). We could obtain the purified DA compound with an overall yield of approximately 78 % using our protocol.

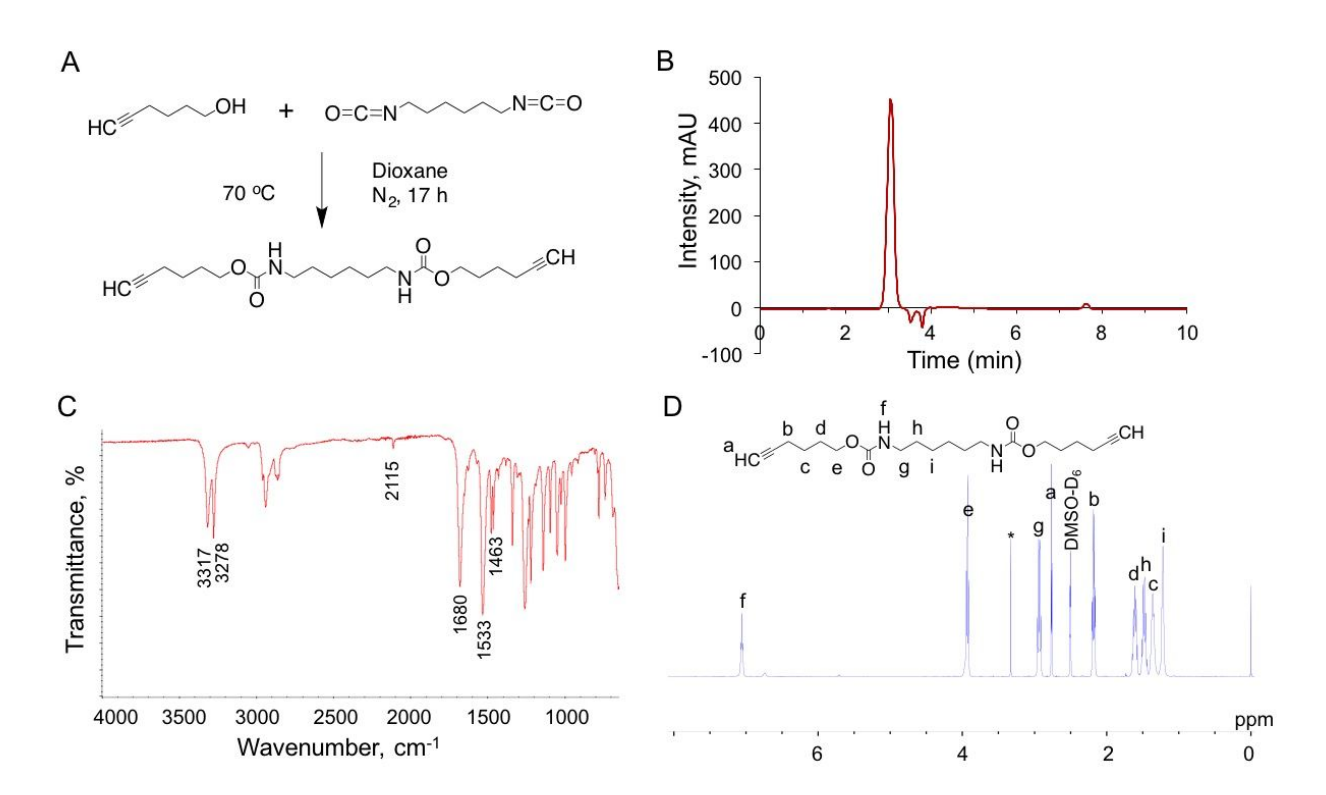


**Figure 2**. (A) Synthesis of the DA crosslinker. The molar ratio of hydroxyl to isocyanate is 1.1 to 1 in the reaction. (B) HPLC analysis indicates the purity of the DA product above 96%. (C) FTIR spectroscopic analysis. The DA compound demonstrates absorptions at 1680, 1533 and 1463 cm<sup>-1</sup> from urethane linkages. A weak absorption at 2115 cm<sup>-1</sup> from the stretching of alkyne carbon-carbon triple bond. (D) Proton NMR analysis to confirm the chemical structure. The integral area ratio of  $H_a: H_f: H_g$  is approximately 1: 1: 2, in agreement with the chemical structure of the DA molecule (**Fig. S2**). '\* marked chemical shift at 3.33 ppm is from the water molecules.

Similarly, the chemical structure of the as-prepared DA crosslinker is verified by FTIR and proton NMR analyses (**Fig. 2C** and **D**). The FTIR absorptions at 3317 and 3278 cm<sup>-1</sup> are assigned to the alkyne carbon-hydrogen ( $\equiv$ C-H) and urethane imide (-N-H) stretches respectively. The weak absorption at 2115 cm<sup>-1</sup> is attributed to carbon-carbon triple bond (-C $\equiv$ C-) stretch. The compound also shows the absorptions at 1680, 1533 and 1463 cm<sup>-1</sup> from the urethane linkages.<sup>31</sup> The proton NMR spectrum demonstrates the  $\delta$ s at 2.76 ppm (H<sub>a</sub>), 2.93 ppm (H<sub>g</sub>) and 7.06 ppm (H<sub>f</sub>). They are attributed to the protons from the alkyne, HDI and urethane linkage, respectively

(**Fig. 2D**). The integral area ratio of  $H_a$ :  $H_f$ :  $H_g$  is approximately 1 : 1 : 2 (**Fig. S2**), in agreement with the chemical structure of the DA molecule. The proton NMR and FTIR characterizations confirmed the successful synthesis of the DA crosslinker.

# 2. Synthesis and characterization of the APU pre-polymer

We copolymerize the BAG monomer and tetraethylene glycol (TEG) with HDI to yield the APU pre-polymer (**Fig. 3A**). 10 mol.% of BAG is reacted with HDI, followed by adding 90 mol.% of TEG to form the resultant APU pre-polymer. In this case, the BAG is randomly incorporated into the APU backbone. The resultant APU is purified by repetitive solvation in dimethylformamide and precipitation in diethyl ether and ethanol/deionized water, followed by additional wash with deionized water with yield of approximately 87% after freeze-drying.

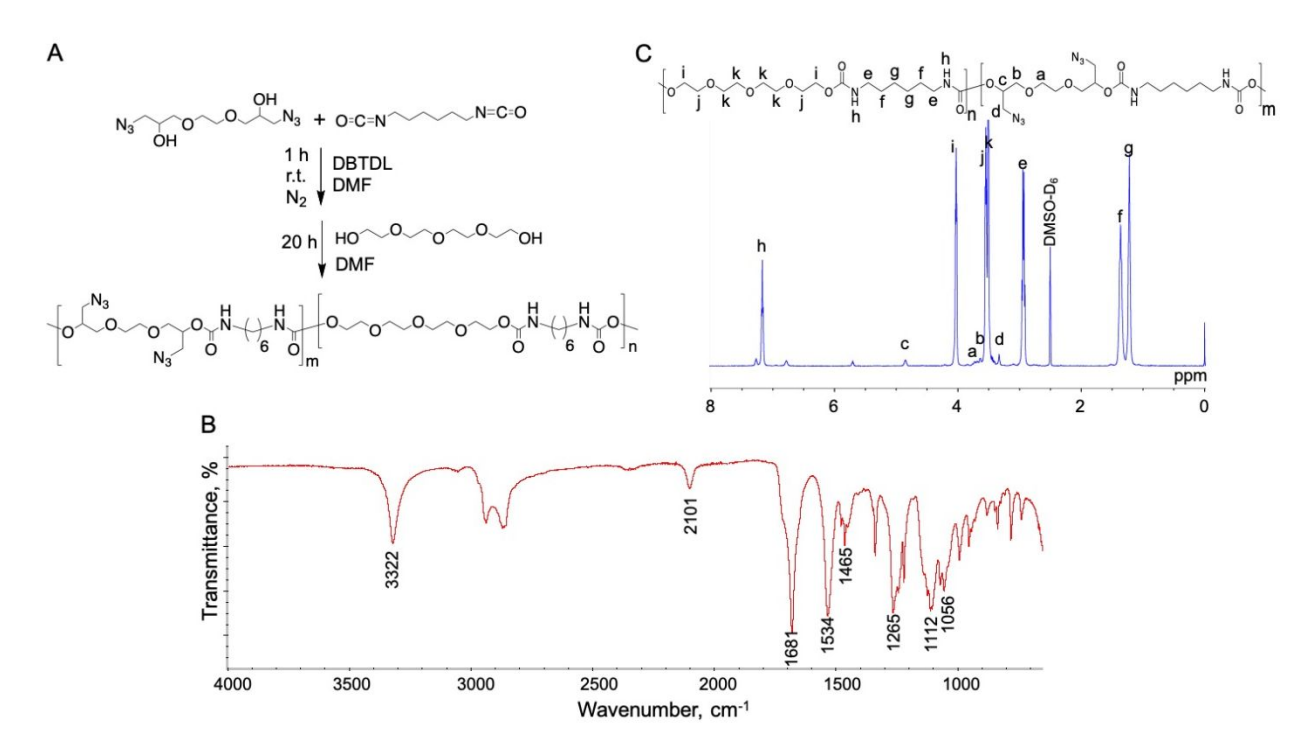


**Figure 3**. (A) Synthesis route of the APU pre-polymer. The theoretic molar ratio of BAG to TEG to HDI is 1:9:10. (B) FTIR analysis of the resultant APU pre-polymer. The spectrum shows absorptions at 3322 cm<sup>-1</sup> from urethane -N-H stretching, and 1681, 1534 and 1465 cm<sup>-1</sup> from urethane linkages. The absorption at 2101 cm<sup>-1</sup> is attributed to the azido groups. (C) Proton NMR analysis of the resultant APU pre-polymer. The NMR spectrum demonstrates chemical shifts from

BAG, TEG and HDI components. The integral area ratio of  $H_d$  to  $H_e$  is used to determine the actual azido content to be approximately 10 mol.% pendent on the polymer backbone (**Fig. S3A**).

The FTIR spectroscopic analysis shows absorptions at 3322 cm<sup>-1</sup> from the urethane imide (-N-H) stretch and the absorptions at 1681, 1534 and 1465 cm<sup>-1</sup> from the stretching of the urethane bonds. Importantly, the spectrum also exhibits the absorption at 2101 cm<sup>-1</sup> in the resultant APU, indicating the presence of azido groups (**Fig. 3B**). The FTIR analysis provides a qualitative evidence for the successful synthesis of the APU pre-polymer.

Proton NMR analysis is performed to further examine the APU chemical structure and composition. The overall  $\delta s$  are correspondingly labeled in **Fig. 3C**. The NMR spectrum shows  $\delta s$ from BAG, TEG and HDI components as well as the urethane linkages formed between them. For example,  $\delta$  at 7.16 ppm is attributed to the urethane imide protons (-N*H*-C=O, H<sub>D</sub>);  $\delta$  at 4.03 ppm is assigned to the methylene protons from TEG (-CHH-O-C=O, H<sub>i</sub>);  $\delta$  at 3.32 ppm is from the azido-methylene protons in BAG ( $N_3$ -CHH-,  $H_d$ );  $\delta$  at 2.95 ppm is assigned to the methylene protons in HDI (-CHH-NH-C=O, H<sub>e</sub>). The integral area ratio of H<sub>d</sub> to H<sub>e</sub> is used to determine the actual azido content to be approximately 10 mol.% in the APU pre-polymer (Fig. S3A). Because one BAG monomer bears two azido groups (Fig. 3A), we can calculate that approximately 5 mol.% of the BAG monomer is incorporated into the APU backbone. Therefore, under the current reaction condition, about 50 % of the BAG monomer was actually reacted with HDI according to the reactant feed ratio. We expect that a longer reaction time between the BAG and HDI is needed before adding the TEG segment if a higher incorporation efficiency of the BAG monomer is desired. This is because the secondary hydroxyl groups in the BAG monomer is less reactive with isocyanate compared with the primary hydroxyl groups in the TEG monomer. To this end, we further examined the reaction efficiency by increasing the reaction time to 3 h between the BAG and HDI before adding the TEG segment. All other reaction conditions remained the same. Proton NMR analysis indicates that approximately 6.6 mol.% of BAG monomer is incorporated into the

resultant APU backbone, indicating 66% of reaction efficiency is achieved under this reaction condition (**Fig. S3B**). These data confirmed the hypothesis that increasing the reaction time between the BAG and HDI could enhance the incorporation efficiency if needed. A higher content of azido pendants can theoretically form more crosslinking points in the resultant APU elastomers to adjust the mechanical properties and elastic deformation profiles. However, because of UV light sensitive and explosive nature of the azido groups,<sup>32</sup> a higher content of azido pendants is not advantageous for material storage and handling. We therefore focus on the APU pre-polymer with 10 mol.% of azido pendants for study in this work.

The molecular weight of the APU pre-polymer is determined by gel permeation chromatography (GPC) (**Fig. S4**). The weight average and number average molecular weights ( $M_w$  and  $M_n$ ) are 21930  $\pm$  1230 Da and 15000  $\pm$  2127 Da with polydispersity (PDI) of 1.47  $\pm$  0.12. Because the material property is typically dominated by high molecular weight polymers, we use the  $M_w$  value to calculate the repeat units and the incorporated BAG molecules per chain. Therefore, according to the molecular weight of the repeat unit and the actual azido content (10 mol.%), the APU pre-polymer is comprised of approximately 56 repeats with 3 to 4 BAG units per chain, namely 6 to 8 azido groups pendent on each chain. These pendent azido groups are responsible for the subsequent click reaction with different amounts of the di-alkyne crosslinker to make APU elastomers.

Because the azido group is thermally instable,<sup>32-33</sup> this might affect the stability of the prepolymer for utility. We therefore examined the material thermal properties by DSC analysis in a
heat-cool-heat model under nitrogen atmosphere with a heating rate at 5 °C/min (**Fig. S5A**). The
DSC test demonstrates five endothermic absorptions at 24, 78, 244, 260 and 310 °C as well as a
minor exothermic peak at around 230 °C in the first heating process from 20 to 450 °C. No thermal
events are observed upon cooling and the second heating process to the same sample. The
sample turned from an initially white powder to a dark brown bulky solid after the DSC test. The
small exothermic peak at around 230 °C is attributed to the decomposition of azido groups.<sup>33</sup> The

heat release is not intensive because of the low azido content (10 mol.%) in the pre-polymer. The other three endothermic events at 244, 260 and 310 °C are attributed to the decomposition of the polyurethane in three steps (**Fig. S5A**). Such polyurethane decomposition profile with three endothermic events was also reported in a literature.<sup>34</sup> The DSC data suggest a considerable thermal stability of the resultant APU pre-polymer at temperature below 200 °C.

To better understand the glass transition temperature  $(T_g)$ , melting temperature  $(T_m)$  and crystallization  $(T_c)$  of the APU pre-polymer, the DSC analysis is performed (**Fig. 4** and **Fig. S5B**). In this case, the maximum temperature is at 200 °C to avoid the decomposition of the pre-polymer. The APU pre-polymer demonstrates an intense  $T_g$  at -11.6 °C and a mild  $T_g$  at 42.4 °C respectively. They are attributed to glass transitions of the amorphous domains formed by soft segments and the low contents of azido-containing hard segments. In addition, the material also shows two melting temperatures at -8.0 °C  $(T_{m1})$  and 81.1 °C  $(T_{m2})$ , and one crystallization temperature  $(T_c)$  at -9.4 °C with an enthalpy of approximately 3.5 J/g from the crystallization process (**Fig. S5B**). According to the above DSC analyses, this APU pre-polymer is a semi-crystalline material with a reversible crystallization feature. For a long-term storage, the APU pre-polymer is suitable to keep in a sealed container at 4 °C and avoid UV light exposure which might induce reactions of the azido groups.<sup>32</sup>

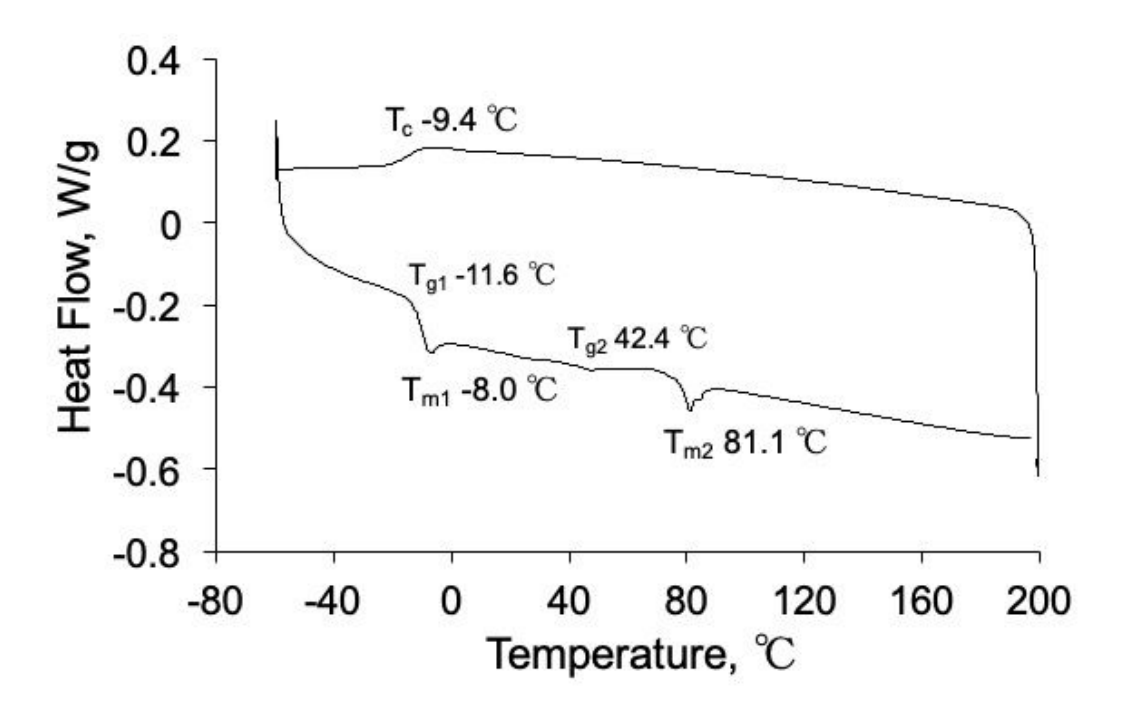


**Figure 4.** DSC analysis of the APU pre-polymer in a heat-cool-heat model under nitrogen flow of 50 ml/min. The thermal profiles from the cooling and second heating are shown here. The APU pre-polymer possesses two  $T_g$ s at -11.6 °C and 42.4 °C, two  $T_m$ s at -8.0 °C and 81.1 °C, and one  $T_c$  at -9.4 °C. The pre-polymer is a semi-crystalline material with a reversible crystallization feature.

3. APU pre-polymer quickly forms stable elastomers by click chemistry

the resultant APU elastomers with porous structure.

# The main objective to design this APU pre-polymer is to easily make PU elastomers using copper(I)-catalyzed azido/alkyne click chemistry under a mild condition. In principle, the asprepared APU elastomer with free azido groups can be further functionalized with any alkyne-bearing moieties for utility. Here, we focus on making APU elastomers by click chemistry for investigation. To this end, we made a series of APU elastomers by crosslinking the pre-polymer solution (20% wt./v in DMF) with different amounts of the DA crosslinker in the presence of copper (I) catalyst (**Fig. 5A**). The click reaction was performed at 37 °C for 4 h to form different APU gels, followed by subsequent wash in DMF/EDTA solution, deionized water and 0.9% saline to obtain

We examined the crosslinking reactions with azido to alkyne molar ratios (Az/Ak) ranged from 1.2 to 0.6 to make the APU elastomers, namely APU-1.2, APU-1.0, APU-0.8 and APU-0.6. The copper (I) catalyzed azido/alkyne click reaction could achieve approximately 85-95% reaction efficiency within hours.<sup>35</sup> Therefore, Az/Ak ratios at 1.0 to 0.8 will yield more densely crosslinked elastomers compared to the Az/Ak ratios at 1.2 and 0.6, and few free azido group will be present on the crosslinked network (Fig. 5A(b)). When making the APU-1.2 elastomer, approximately 20% of azido groups are free from the crosslinking reaction, resulting in a lower crosslinking density (Fig. 5A(a)). Given the actual 10 mol.% of azido groups in the APU pre-polymer (Fig. 3), there are approximately 2 mol.% of free azido groups pendent on the APU-1.2 networks (Fig. 5A(a)). When Az/Ak ratio at 0.6, the reaction also leads to a lower crosslinking density in the APU-0.6 likely with some unreacted alkyne groups pendent on the networks (Fig. 5A(c)). However, there are some unreacted DA residues as well because the click reaction efficiency is less than 100%. We expect the mechanical properties will accordingly change as the Az/Ak ratios alter for the crosslinking to make these elastomers. In addition, regardless of the different Az/Ak ratios for crosslinking, we would like all elastomers to be stable enough for reversible mechanical deformations. To examine the elastic performance, cyclic tensile tests are first performed to evaluate the elasticity and the ability to recover from the reversible mechanical deformations (Fig. 5B-E).

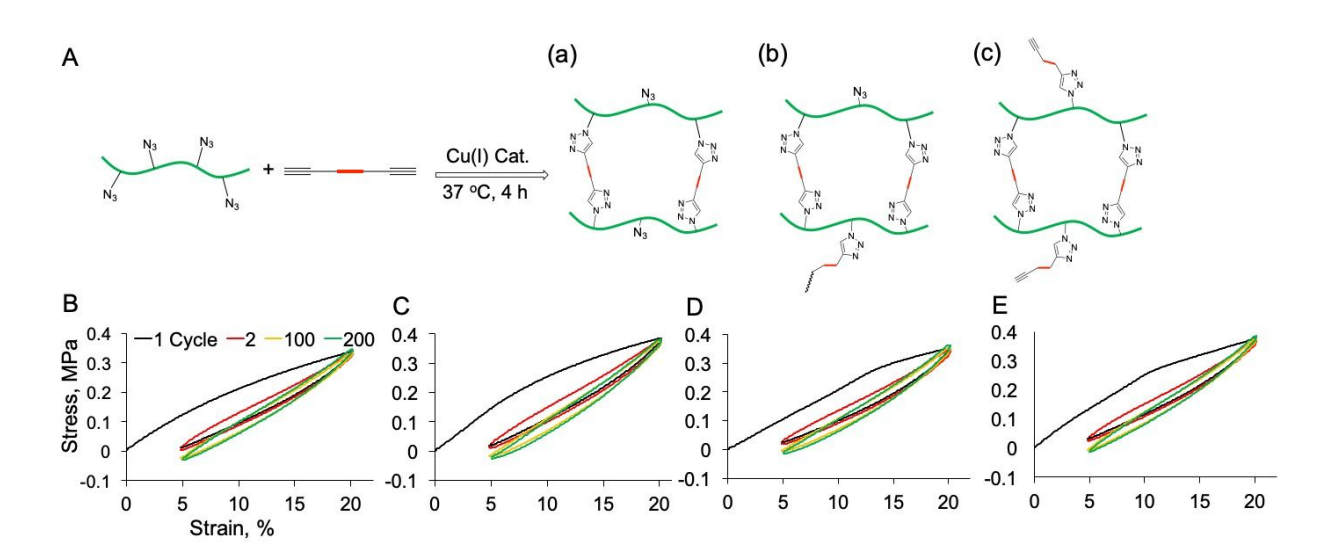


**Figure 5**. (A) Schematic illustration of the APU pre-polymer crosslinked with DA crosslinker by copper(I) catalyzed click chemistry. (a) Az/Ak ratio > 1.0, free azido groups; (b) Az/Ak ratio = 1.0 to 0.8, few free azido or alkyne groups; (c) Az/Ak ratio < 0.8, free alkyne groups. (B-E) Cyclic tensile tests to examine the elasticity and the abilities for reversible elastic deformations. (n = 3) (B) APU-1.2, (C) APU-1.0, (D) APU-0.8 and (E) APU-0.6. All elastomers demonstrated similar elastic deformation profiles and could undergo at least 200 cyclic loading without break, indicating highly stable polymeric networks within the strain range tested.

Here, all APU elastomers are prepared with porous structure and soaked in 0.9% saline before the mechanical tests given the biological setting. The cyclic tensile test is limited to 200 cycles to avoid excessive water evaporation that will lower the consistency of test conditions. Notably, all elastomers can undergo reversible elastic deformations between 5 and 20% strain for at least 200 cycles without break. These elastomers demonstrate similar reversible deformation profiles (**Fig. 5B-E**). The first two cycles led to relatively large hysteresis loops among them, indicating somewhat damages in the polymeric networks. We speculate that the damages at this stage mainly occur in some physically entangled or interacted polymer chains, which are not reversible and easily disrupted by the loading force. In the following cyclic loading, the hysteresis loops remain nearly identical to the second cycle across the cyclic tensile tests, suggesting little

further damage occurred in the polymer networks. The exerted stress from the cyclic loading is efficiently dissipated by the reversible interactions between the polymer chains, including the hydrogen bonds formed between the urethane linkages. Such elastic performance is very important for an elastomeric scaffold in biomedical applications. For example, when fabricating polyurethane scaffolds for myocardial tissue engineering, robust elasticity is highly desired to retain the heart patch integrity for mechanical support and thus improve the treatment efficacy. <sup>15</sup>. <sup>36-38</sup> We would like to note that all of these APU elastomers demonstrate a stable network structure for reversible deformations within the strain range tested, regardless of the different Az/Ak ratios for crosslinking. We examined the deformations within 20% strain, which is a typical range of biomechanical deformations for many soft tissues. <sup>39-40</sup> In addition, if the APU elastomer needs to be further functionalized with biomolecules in a design, the APU-1.2 can be used for this purpose as the FTIR analysis confirmed the presence of free azido groups (**Fig. S6**). Less crosslink does not compromise its elastic performance for utility.

We further investigated other mechanical properties including the strain at break, ultimate tensile strength (UTS) and Young's modulus (E) using uniaxial tensile test (**Fig. 6**). All elastomers demonstrate an elastic elongation until break (**Fig. 6A**). As we expected, when the crosslinking density increases, the strain at break decreases and the E elevates. These phenomena are typically seen in chemically crosslinked elastomers. In our case, the APU-1.2 and APU-0.6 are less crosslinked than the APU-1.0 and APU-0.8, they therefore show a longer elongation at break; the APU-0.6 is most stretchable among them (\*p = 0.0331, **Fig. 6B**). On the other hand, the E values increase in the APU-1.0 and APU-0.8 because of the higher crosslinking density compared to the APU-1.2 and APU-0.6 (**Fig. 6D**). For all of these elastomers, the UTS values range from  $562 \pm 53$  kPa to  $647 \pm 49$  kPa, showing no significant difference (**Fig. 6C**). The APU-0.8 and APU-1.0 show similar strain at break and E values, indicating a very close crosslinking density between them given the actual azido/alkyne reaction efficiency.

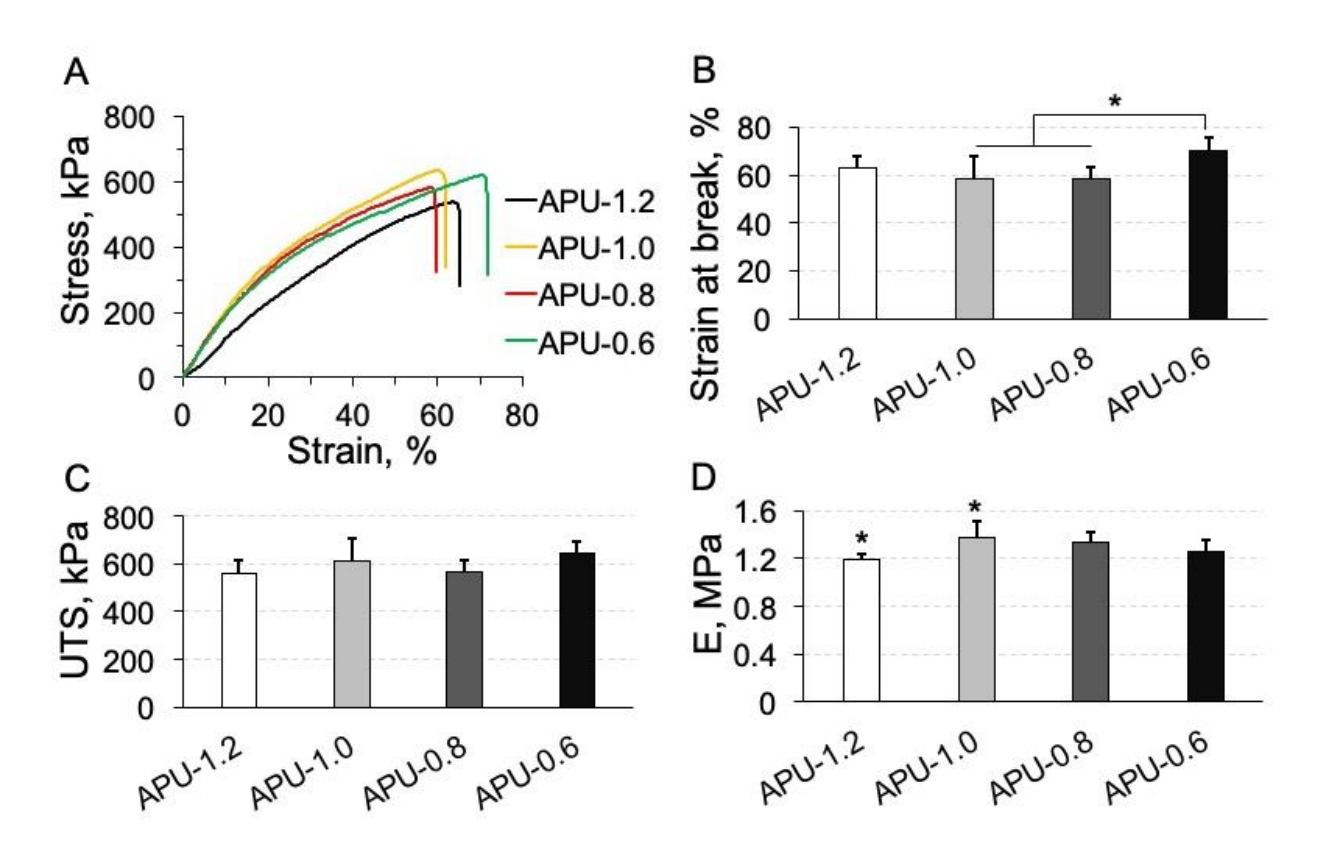


**Figure 6**. (A) Representative stress-strain curves of APU elastomers made with Az/Ak molar ratios ranged from 1.2 to 0.6. The mechanical properties are compared: (B) strain at break (\*p = 0.0331), (C) UTS (p = 0.1620) and (D) E (\*p = 0.0467). Generally, when the Az/Ak ratio approaches to 1.0 for crosslinking, the elastomer demonstrates an increased E and decreased strain at break. One-way ANOVA analysis with Tukey post-test is performed for statistical analysis. Data represents the mean  $\pm$  SD (n = 5).

Although the Young's moduli demonstrate differences along with the crosslinking density, they only range from  $1.20 \pm 0.05$  MPa for the APU-1.2 to  $1.38 \pm 0.13$  MPa for the APU-1.0 (\*p = 0.0467, **Fig. 6D**). This scope is very limited to adjust through the crosslinking reactions. We therefore further examined the impacts of the APU pre-polymer concentrations on the mechanical properties of the resultant elastomers.

We compare the APU pre-polymer concentrations at 10, 20 and 30% wt./v in DMF while the Az/Ak ratio is remained at 1.2 for crosslinking to make the elastomers. They are designated

as APU-10%, APU-20% and APU-30%. Changing the pre-polymer concentration would alter the density of polymer chains and hydrogen bonds between the urethane linkages, the chain-chain interaction patterns and the network porosity. Thus, the mechanical properties are expected to be further tunable (**Fig. 7**).

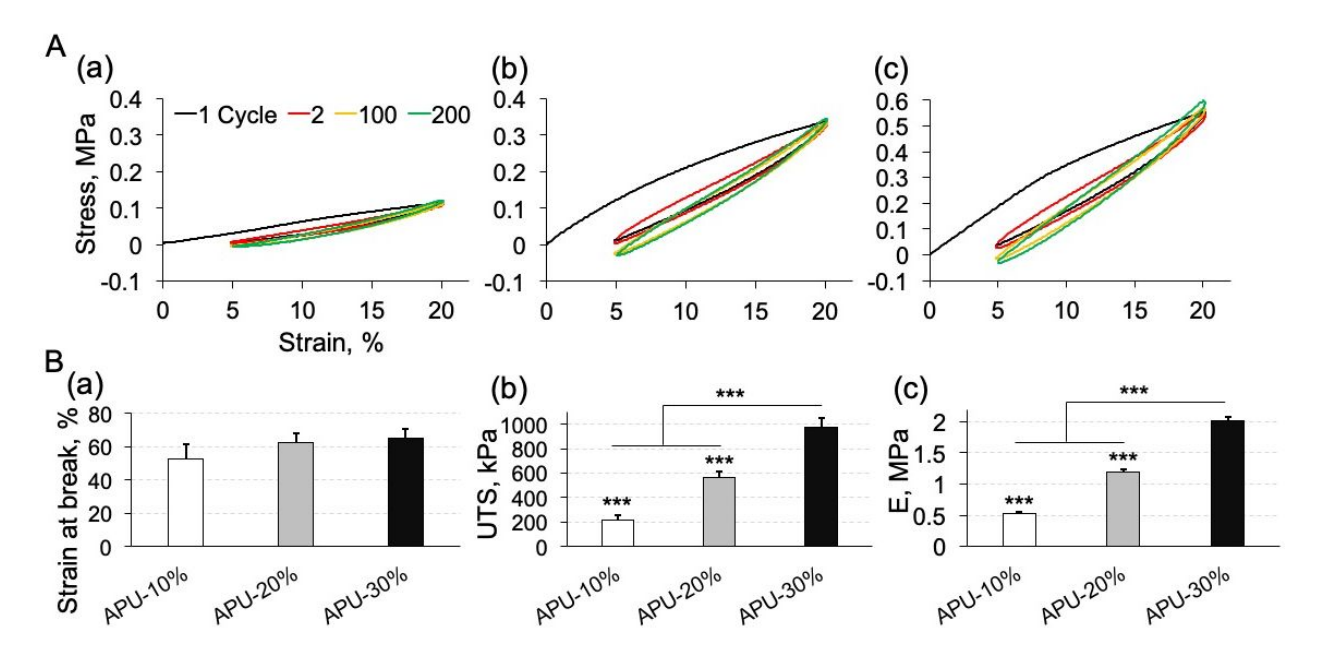


**Figure 7**. (A) Cyclic tensile tests to examine the elasticity and the ability for reversible elastic deformations (n = 3). (a) APU-10%, (b) APU-20%, (c) APU-30%. All elastomers could undergo at least 200 cyclic loading without break. The lower pre-polymer concentration yields a softer elastomer with a smaller hysteresis loop, indicating less network damages. (B) Comparison of the mechanical properties. (a) Strain at break (\* p = 0.0342) (b) UTS (\*\*\* p < 0.0001), (c) E (\*\*\* p < 0.0001). The pre-polymer concentrations could significantly affect the UTS and E values of the elastomers, but slightly the strain at break. One-way ANOVA analysis with post-test of Bonferroni is performed for the statistical analysis. Data represents the mean ± SD (n ≥ 4).

Similarly, we performed cyclic tensile tests to examine the elasticity and the ability to recover from reversible mechanical deformations (**Fig. 7A**). All elastomers could undergo reversible elastic deformations without break across the 200 cyclic loading within 20% strain. However, their deformation profiles are apparently different. The APU-10% is much softer than

the APU-20% and APU-30%, and thus demonstrates a smaller hysteresis loop, indicating less damages of the polymer networks by the cyclic loading. Both the UTS and E values demonstrate significant differences among them (**Fig. 7B**). The E value elevates from  $0.52 \pm 0.03$  MPa to  $2.02 \pm 0.07$  MPa and the UTS ranges from  $213.3 \pm 46.3$  kPa to  $971.2 \pm 75$  kPa as the pre-polymer concentrations increase from 10 % to 30 % wt./v to make the elastomers. On the other hand, when the Az/Ak ratio is remained at 1.2 for crosslinking in the three elastomers, a reduction of the APU pre-polymer concentration only slightly compromises the strain at break. These mechanical properties suggest this material is suitable to design different elastomeric scaffolds for different applications by easily adjusting the pre-polymer concentration for crosslinking. In addition, we anticipate the presence of free azido groups would be useful in the elastomeric scaffold designs. We therefore mainly examined the mechanical properties of these porous elastomers with the Az/Ak ratio remained at 1.2 for the crosslinking.

To examine the mechanical properties of APU in a compact form, porous APU-1.2 sheets were freeze-dried and compressed to fuse at 80 °C for 30 min to form compact APU-1.2 samples. The cyclic tensile test is performed for 1000 cycles with 20 % strain to evaluate the elasticity. Water evaporation is minimized and do not interfere the reversible deformations throughout the cyclic tensile test. The elastic deformations and mechanical properties are compared with two commercially resourced catheter materials, PVC and Nylon-12 (**Fig. 8**). They are selected for comparison because the PVC and Nylon-12 are typical thermoplastics with low and high Young's modulus and widely used to make medical devices including the catheters.<sup>42</sup> The PVC is a relatively soft elastomer that is able to undergo a linear elongation with E of  $5.6 \pm 0.3$  MPa and strain at break up to  $376 \pm 48\%$ . Nylon-12 is a relatively stiff plastic with E of  $456 \pm 20$  MPa during an elastic elongation of approximately 6% strain, followed by a plastic deformation with a strain at break of  $183 \pm 29\%$  (**Fig. 8B**). The cyclic tensile tests indicate that the PVC shows relatively small hysteresis loops with a slight permanent elongation across the 1000 cyclic loading, indicating a mild network damage. However, the Nylon-12 exhibits a permanent elongation of

approximately 13% strain with relatively large hysteresis loops after 1000 cyclic loading, indicating a severe network damage and a permanent deformation by the loading stress (Fig. 8A). Compared to the PVC and Nylon-12, the compact APU-1.2 elastomer is able to undergo elastic elongation with a strain at break of  $150 \pm 13\%$  that is comparable to the Nylon-12 (Fig. 8B(b)). The reversible elastic deformations are more like the PVC at the early stage with similarly small hysteresis loops (Fig. 8A(a, b)). The first two hysteresis loops without a permanent elongation are mainly attributed to the disruption of the irreversible physical interactions, which is similar to the wet porous APU-1.2 elastomer demonstrated (Fig. 5B). However, because no water molecules act as plasticizer in the compact APU-1.2 elastomer, thus the polymer chain mobility and reversible interactions between the polymer chains are compromised. As a result, the exerted stress by the cyclic loading cannot be efficiently dissipated. Therefore, as the cyclic loading increases, damages accordingly occur in the compact APU-1.2 networks. A permanent elongation reaches approximately 10% strain after 1000 cyclic loading, but is milder than that of the Nylon-12 (Fig. 8A(a, c)). The cyclic tensile tests suggest that the compact APU-1.2 elastomer possesses elastic performance between the PVC and Nylon-12 resins. Other mechanical properties are further examined by uniaxial tensile tests (Fig. 8B).

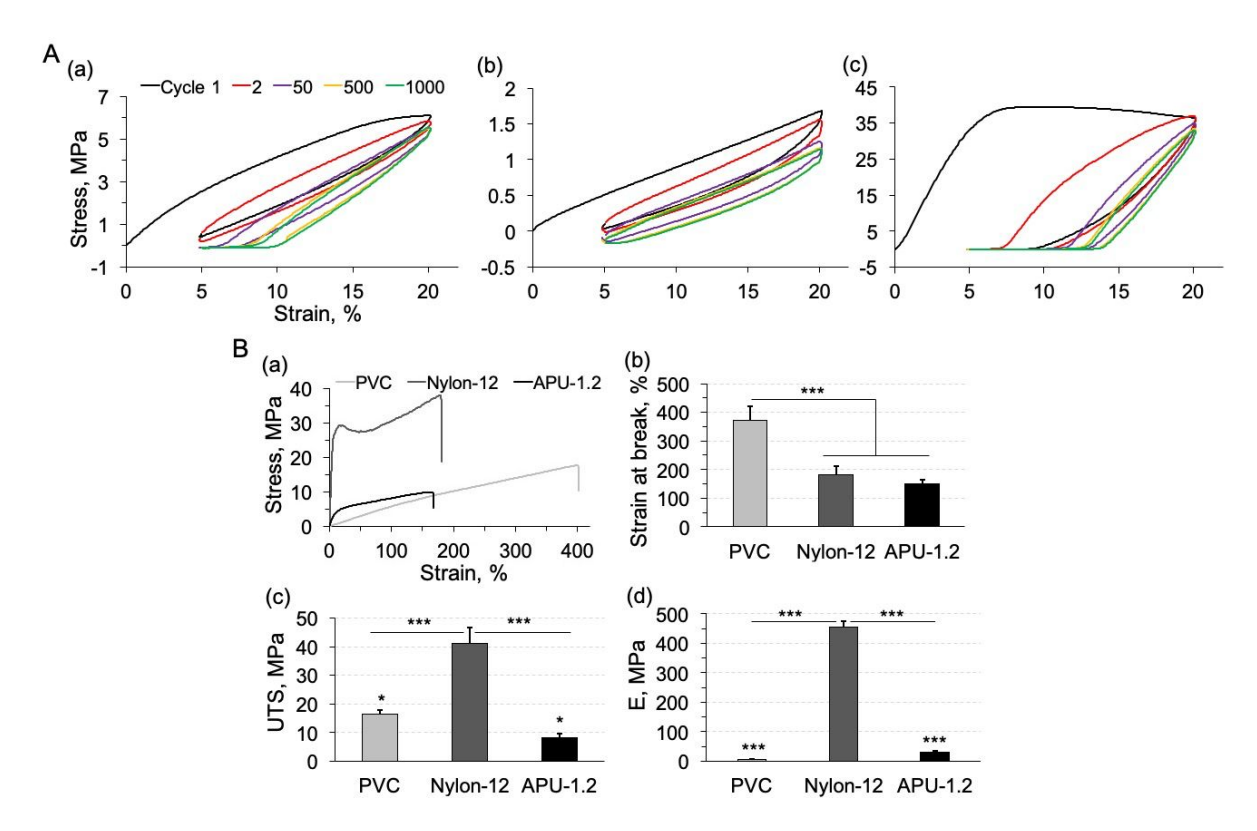


**Figure 8**. (A) Cyclic tensile tests to compare the elastic performances (n = 3). (a) Compact APU-1.2, (b) PVC, (c) Nylon-12. Compared to the PVC and Nylon-12, the compact APU-1.2 elastomer is more like the PVC for reversible elastic deformations at the early stage. As the cyclic loading goes up to 1000 cycles, the APU-1.2 shows a permanent elongation of approximately 10% strain, indicating some network damages but less severe than Nylon-12. (B) Comparison of the mechanical properties. (a) Representative stress-strain curves of PVC, Nylon-12 and APU-1.2, (b) strain at break (\*\*\* p < 0.0001), (c) UTS (\*\*\* p < 0.0001) and (d) E (\*\*\* p < 0.0001). The compact APU-1.2 elastomer shows a strain at break comparable to the Nylon-12. The E at 0-15% strain reaches 28.8 ± 5.2 MPa, nearly 5 times to that of the PVC. One-way ANOVA analysis with Bonferroni post-test is performed for the statistical analysis. Data represents the mean ± SD (n = 4).

The uniaxial tensile tests indicate that the compact APU-1.2 demonstrates two elastic elongation regions at 0 to 15% strain and 25% strain to break with a curved region between 15% and 25% strain. The E values transit from an initially high modulus of  $28.8 \pm 5.2$  MPa (0-15%)

strain) to a relatively low modulus of 3.0 ± 0.4 MPa (25% strain - break) (Fig. 8B). Such elastic elongation profile with a transition region is apparently different with the typical plastic deformation with a yield stress as the Nylon-12 demonstrated (Fig. 8B(a)). We speculate that the unique elastic elongation is mainly caused by different crosslinking densities, different polymer chain length between the crosslinks and some irreversible physical interactions in the compact APU-1.2 elastomer. This is because the azido pendants are randomly distributed along the APU prepolymer for crosslinking to form the APU-1.2 elastomer. Therefore, at the early phase of the elongation, the high crosslinking domains with short polymer chains dominate the high E value under stretching (0-15% strain). As the elongation continues to 15% - 25% strain, the tightly crosslinked polymer networks are gradually broken and thus E value accordingly transits to the low modulus region (25% strain - break) for elongation. In addition, some irreversible physical interactions also contribute to the crosslinks and the high E value that are disrupted at the early stage during the stretching. This is evidenced by the above cyclic tensile tests and DSC analysis of the compact APU-1.2 elastomer (Fig. 8A, Fig. S5C). The DSC analysis shows a melting temperature at 75.3 °C with an endothermic enthalpy of 25.6 J/g during the first heating, indicating the presence of crystalline structures. However, no similar endothermic event is observed in the second heating, except a glass transition temperature at approximately -8.9 °C. The cooling process demonstrates a mild exothermic enthalpy of 5.7J/g at -6.8 °C, indicating only a partial crystallization occurred. These DSC data suggest that most of the crystalline structures are not reversible because of the limited chain mobility for crystallization during the cooling process in the crosslinked compact APU-1.2 networks. Therefore, the crystalline domains contribute to the crosslinking points and the E value at the early stage of elongation. Compared to the wet porous APU-1.2 elastomer that does not show a curved transition region between 15% and 25% strain upon elongation (Fig. 6), we speculate that the irreversible crystalline crosslinks are mainly responsible for this curved transition region in the compact APU-1.2 elastomer. Based on the above analyses, it appears that the distribution and the numbers of the azido pendants along the

APU backbone can be further adjusted to mediate the crosslinking density, the uniformity of chain length between the crosslinks and the elastic deformation profiles.

Because the Nylon-12 only demonstrates an elastic elongation of approximately 6% strain, the E value at 0-15% strain of the compact APU-1.2 elastomer is used to compare with those of the PVC and Nylon-12. The modulus of the APU-1.2 is nearly five times to that of the PVC, but only one sixteenth to that of the Nylon-12. The UTS reaches  $8.2 \pm 1.3$  MPa, which is smaller than both the PVC ( $16.7 \pm 1.6$  MPa) and the Nylon-12 ( $41.2 \pm 5.5$  MPa). Here, we only examined the mechanical properties of the compact APU-1.2 elastomer and compared with the commercial PVC and Nylon-12 materials. Like the porous APU elastomers, changes of the crosslinking densities can also modulate the E, UTS and strain at break of the compact APU elastomers. Overall, although this APU elastomer is not as tough as the PVC and Nylon-12 resins, its versatile elastic performance with a wide range of tunable modulus makes this material attractive to design stable elastomeric components.

# 4. In vitro degradation

We examined the degradation of the compact APU-1.2 elastomer over 6 days in a 60 mM NaOH solution at 37 °C (**Fig. 9**). For comparison, a biodegradable poly(glycerol sebacate) elastomer similarly with a compact structure demonstrated  $23.1 \pm 1.6\%$  degradation over 3 days under the same testing condition . To this stable APU elastomer, the degradations of all groups are remained below  $1.9 \pm 0.7\%$  across the experimental window, demonstrating a considerable stability under this testing condition. An *in vivo* subcutaneous implantation study in mice indicates similar stability of the samples during the 8 weeks test window (Supporting Information, **Fig. S7**).

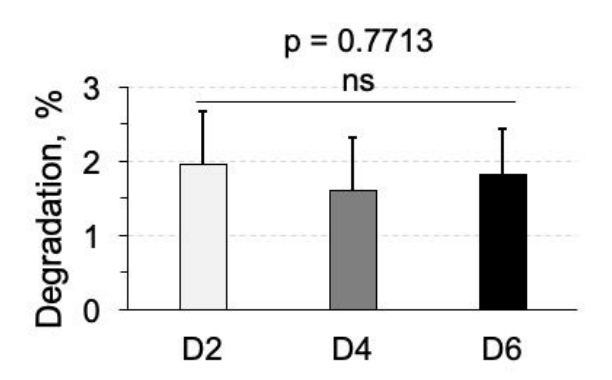


**Figure 9**. *In vitro* degradation of the APU-1.2 elastomer in a 60 mM NaOH solution at 37 °C over different times. The degradation is remained below  $1.9 \pm 0.7\%$  across the experimental window, showing a considerable stability against basic erosion. One-way ANOVA analysis with Bonferroni post-test is performed for the statistical analysis. Data represents the mean  $\pm$  SD (n = 4).

# 5. *In vivo* biocompatibility

Currently, we focus on making the APU elastomers without any further functionalization, we therefore selected the APU-1.0 elastomer for *in vivo* biocompatibility study. Disc samples with diameter of approximately 6 mm and 1 mm in thickness were punched from an elastomeric sheet and sterilized by autoclave for implantation. The disc samples were subcutaneously implanted in mice backs over 56 days to investigate the host responses. All animals survived throughout the experiments without any infection or abscess at the implanted sites. All implants demonstrated no degradation or surface erosion across the experimental time, demonstrating a considerable biostability (**Fig. S7**).

At days 3, 28 and 56, tissues along with the implants were harvested, sectioned and stained with hematoxylin and eosin (H&E) and Masson's trichrome (MTS) for histological studies. Tissues around the implants show mild adverse responses such as inflammation and fibrosis, but no necrosis or muscle degeneration (**Fig. 10, 11**). H&E staining shows mild phagocytic inflammatory infiltrates near the implants at days 3 post-implantation (**Fig. 10A, D**). The inflammatory infiltrates increase around the implant at days 28, but no cells can infiltrate the implant because of no open pores on the implant surface for cell infiltration (**Fig. 10B, E**). At days

56 post-implantation, the implants remain intact with smooth surface and no erosion occurs. Few cells could attach the implant surface and form foreign body giant cells. The cell population around the implant appears steady compared to that of 28 days (**Fig. 10E**, **F**). However, the extracellular matrix (ECM) deposition around the implant turns into a denser porous structure. It is worth noting that the native tissue alignment and muscle cell morphologies remain the same, indicating no toxins leached from the implants to affect the native tissues.

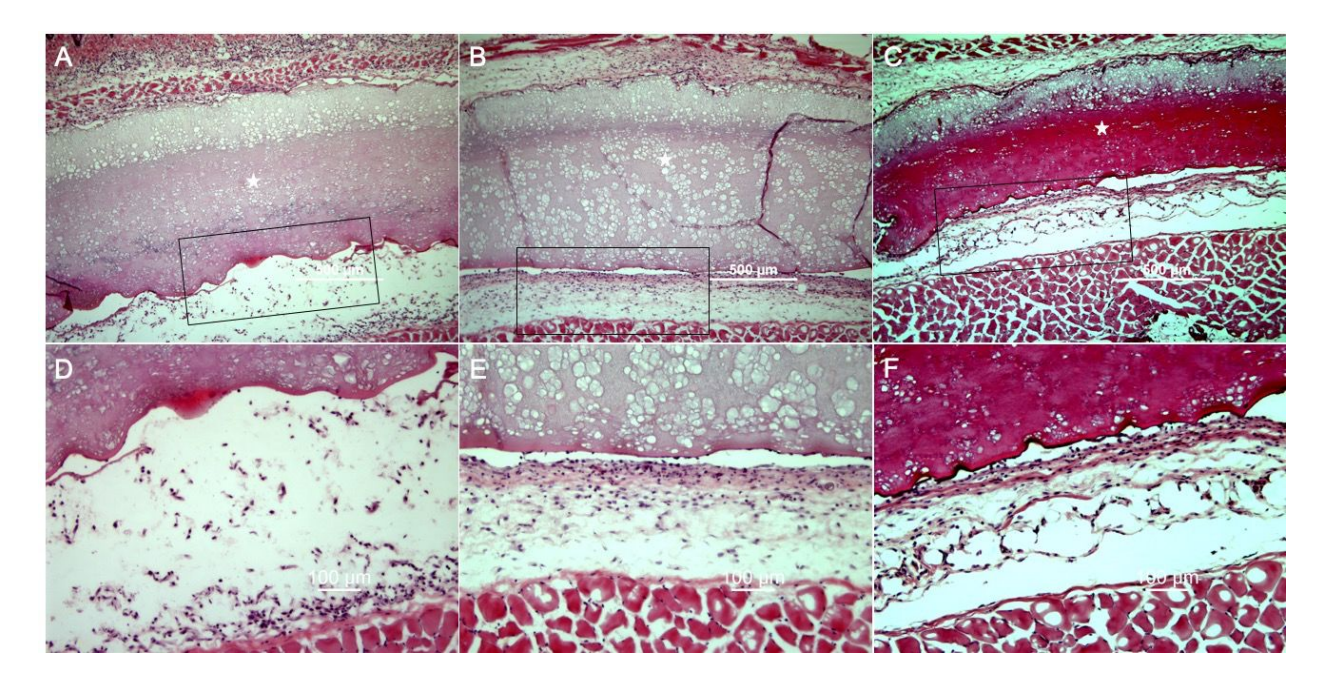


**Figure 10**. Representative micrographs of H&E stained sections surrounding the implants. White star marks the implants. Low magnification of images (A, B and C) represent the H&E stained tissues harvested at days 3, 28 and 56 post-implantation respectively, (Scale bar, 500  $\mu$ m). Rectangular frames indicate the regions chosen for a higher magnification (D, E and F), (Scale bar, 100  $\mu$ m).

We further examined the collagen deposition around the implants by MTS staining. The MTS stained sections show a loose layer of collagen surrounding the implant (blue fibrous structure) at days 28 (**Fig. 11A**, **C**). The collagen deposition becomes a denser and porous capsule to isolate the implant from the surrounding tissue at days 56 (**Fig. 11B**, **D**). This is consistent with what we observed in H&E stained sections (**Fig. 10E**, **F**). When comparing the

collagen thickness over the implantation time, it shows no statistical difference between the days 56 and 28 (**Fig. 11E**). The collagen capsule prevents the recruited cells from approaching the implant, which likely further contributes to the material stability against biological degradation and reduce foreign body reactions.

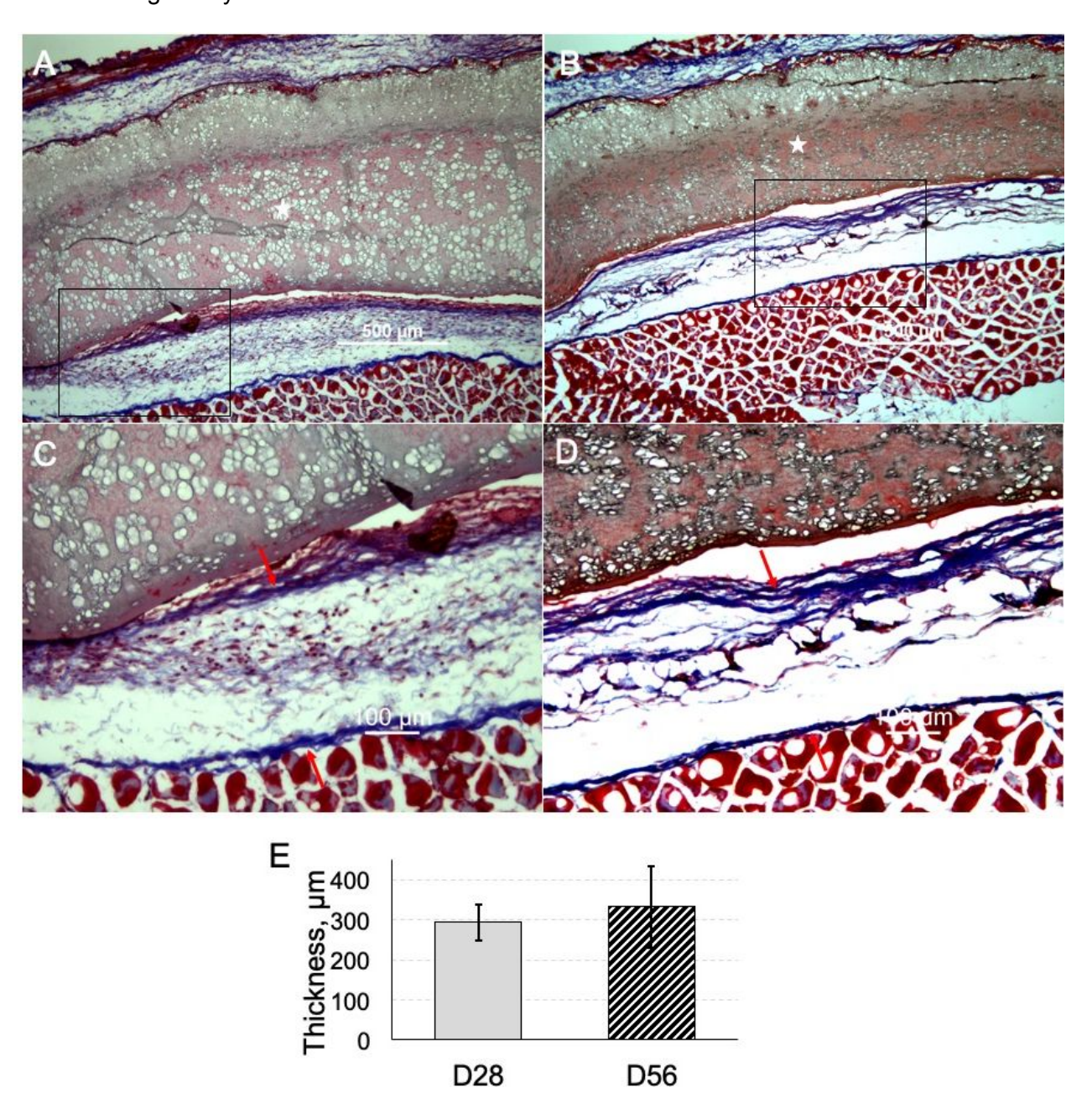


**Figure 11**. Representative MTS stained sections illustrate the collagen deposition around the APU implant over implantation time. The white stars mark the implants. Low magnification of

images (A and B) are the tissues harvested at days 28 and 56 post-implantation (Scale bar, 500  $\mu$ m). Rectangular frames indicate the regions chosen for a higher magnification (C and D), (Scale bar, 100  $\mu$ m). (E) The thickness of collagen deposition around the implants is quantified for comparison at days 28 and 56 post-implantation. To each group, twelve locations around the implants are randomly selected from three MTS stained micrographics to measure the thickness and obtain the mean value with a standard deviation. Red arrow indicates one location as an example for collagen thickness measurement. One-way ANOVA with Bonferroni post-test is used for statistical analysis. A p value < 0.05 is considered significantly different. Data represent the mean  $\pm$  SD (n = 12).

To further investigate the host reactions and cell activities, we use CD68 and DAPI to detect macrophage distribution around the implants (**Fig. 12**). CD68 is a pan-macrophage marker. By days 3 post-implantation, the implants induce a non-specific inflammatory response and recruit immune cells to the implantation site as revealed by CD68 staining (**Fig. 12A**). At days 28 after implantation, the macrophages further increase around the implants compared to days 3, indicating more inflammatory cells are recruited to the implantation site (**Fig. 12B**). The macrophages are then significantly reduced to a level close to that of the contralateral control at days 56 post-implantation (**Fig. 12C-E**), indicating that the inflammation to the material is nearly resolved at this time point. The change of macrophage numbers over the implantation time is consistent with the process of fibrotic encapsulation of the implant. Thus, the inflammatory response further evidenced that the fibrotic capsule indeed reduced the foreign body reactions to the material.

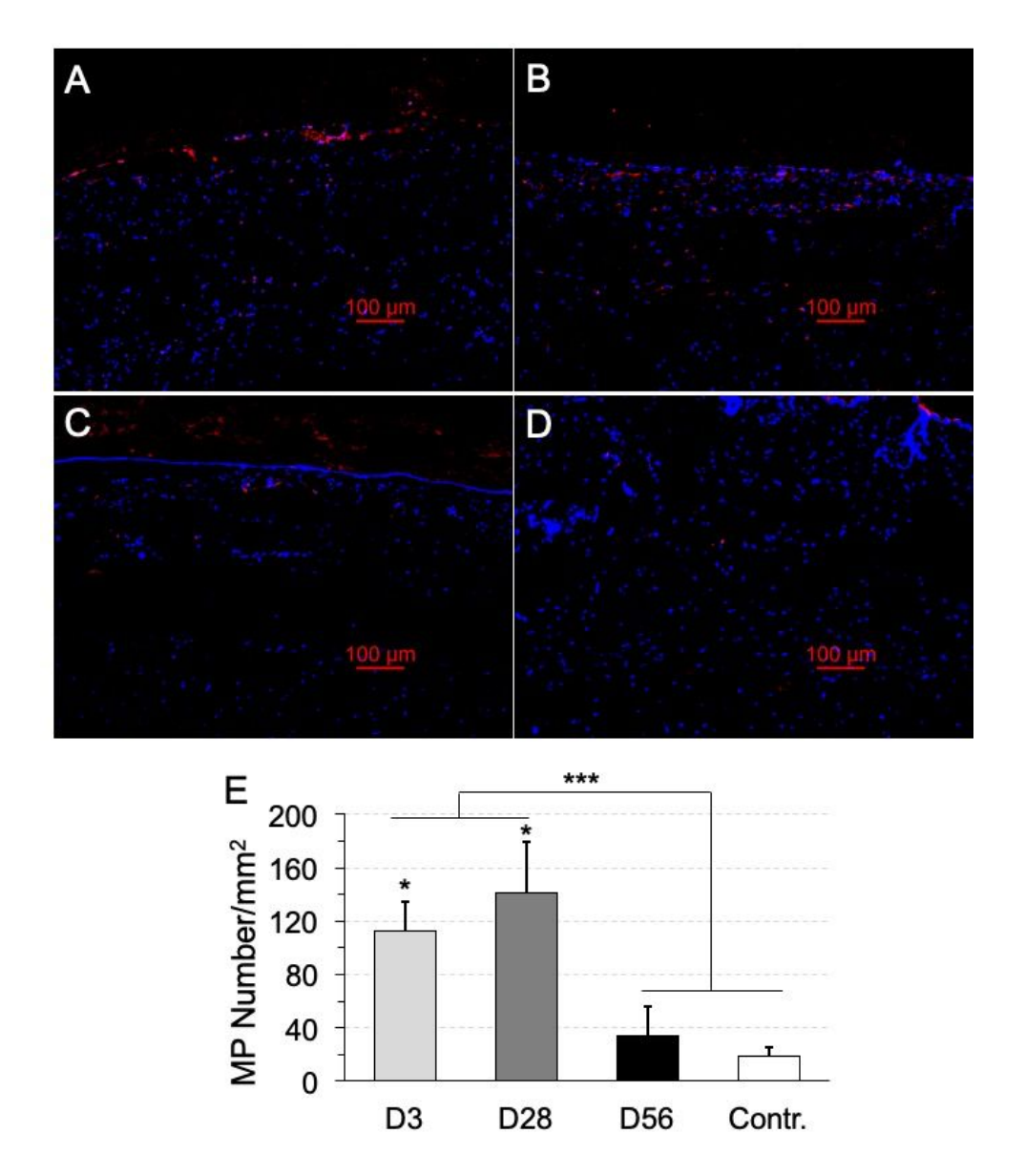


Figure 12. Representative micrographs of immunohistochemically stained sections of CD68 positive macrophages merged with DAPI staining (Scale bar, 100 μm). Tissues were harvested at days (A) 3, (B) 28, (C) 56 and (D) the contralateral tissue at days 56 without implant as a control. The dark areas without DAPI in the images A-C are the implant locations. Some red spots are attributed to the background fluorescence from the absorbed CD68 stain on the implants. (E) Quantification of CD68 positive macrophages (MP number per mm²) at different time points. The population of CD68 positive cells increases from days 3 to 28 post-implantation with a statistical difference. The macrophages then significantly reduce to a level close to the contralateral control

at days 56 post-implantation. Images from more than 9 random areas around the implantation sites are selected for quantification. \*\*\* p < 0.0001. P < 0.05 is considered significant different. Data represent mean  $\pm$  SD (n  $\geq$  9).

Generally, a biomaterial implant in living tissue will activate and recruit the immune cells such as neutrophils, monocytes and macrophages to the implantation site.<sup>39, 43-44</sup> The recruited cells are induced to secrete inflammatory cytokines and chemokines to recruit more immune cells to degrade the foreign material.44 In this case, the elastomeric implant is made with smooth surface and isolated pores. No erosion occurs on the implant surface after implantation. This is different with the reported surface degradation phenomena on the ether-based PU implants. 45-46 We speculate that such difference is likely because of the different implantation time, elastomer structure, crosslinking bonds and ether segment properties of our APU implant. The recruited cells approach the implant, but could not infiltrate it because of no pathway to allow infiltration (Fig. 10). The recruited cells secrete ECM around the implant over time. At days 56 postimplantation, the collagen deposition is densified to become a fibrotic capsule surrounding the implant (Fig. 11). Most of the recruited cells are confined in the capsule layer (Fig. 10C, F). The fibrotic encapsulation contributes to isolate the implant from surrounding tissues and thus reduce the foreign body reactions (Fig. 12). The cell population remains relatively steady across the implantation time. No other adverse host responses were observed after implantation. Overall, the in vivo studies suggest the suitability of this material to construct a stable elastomeric scaffold for tissue engineering applications.

Compared to conventional PU elastomers made from polyol and polyisocyanate,<sup>1</sup> we introduce azido functionality to make the APU elastomers using click chemistry without causing other side reactions. Currently, we selected TEG as an ether diol segment together with the designed BAG monomer to make the APU elastomers. We expect this method to be similarly versatile to make other biodegradable APUs by selecting a polyester based diol as a segment to react with HDI and the BAG monomer. In addition, current method formed isolated pores in the

APU elastomers with smooth surface. No cells could infiltrate the implant. The pore interconnectivity is another important aspect that needs to be improved if an interconnected porous APU scaffold is needed to make a tissue scaffold that could allow cell infiltration and proliferation along with the scaffold.

#### Conclusion

We have reported an APU pre-polymer using a newly designed azido-bearing diol monomer to introduce azido functionality for click crosslinking under a mild condition. This pre-polymer could easily generate stable porous elastomers with tunable mechanical properties through adjusting the azido/alkyne ratios or the pre-polymer concentrations for crosslinking. In addition, this material can also easily form a thermoset elastomer by a compressive heat treatment at a temperature close to its melting temperature. These APU elastomers with different structures therefore possess a wide range of modulus and elastic performance for different utilities. The elastomer showed a considerable stability against erosion in a basic solution. The elastomeric scaffold also demonstrated a considerable biostability as revealed by the subcutaneous implantation study. The implant induced only mild inflammatory responses and fibrotic capsules around the implant. No other adverse host responses were observed. Although we only examined the feasibility using the designed BAG monomer to make an azido-functionalized PU for utility. We believe this monomer can also react with HDI together with other diol segments to manipulate the physical, chemical and biological properties of the resultant APUs for specific applications.

#### **Experimental Methods**

# 1. Synthesis of bisazido diol monomer

All chemicals were used as received. The bisazido diol monomer was synthesized by ring opening reaction between ethylene glycol diglycidyl ether (EGDE) and sodium azide using a reported protocol with modification.<sup>30</sup> Specifically, EGDE (1.742 g, 10 mmol, ~90%, Pfaltz&Bauer Inc, CT, USA) was mixed with 10 ml of CH<sub>3</sub>CN:H<sub>2</sub>O (9:1 v/v). Then Oxone® monopersulfate (Alfa

Aesar) (6.15 g, 10 mmol) was added as catalyst under magnetic stirring for 5 min. Next, sodium azide (99.0%, EMD™) (1.30 g, 20 mmol) was added to the mixture and stirred for 30 min, followed by adding another 1.30 g of sodium azide and 1.0 ml of deionized water. The reaction was remained for 44 h under nitrogen atmosphere with gentle magnetic stirring to yield a light yellowish solution with sediments. The mixture was rot-evaporated under reduced pressure (50 mmHg) at 25 °C for approximately 2 h to remove solvent. The solid residues were then extracted with 4×30 ml dichloromethane (DCM) and the organic layers containing raw product were combined, followed by adding sodium sulfate anhydrous (25 g) to dry overnight. The organic layer was then decanted into another flask and rot-evaporated under reduced pressure at 50 °C for about 2 h to remove DCM. A raw product of the bisazido diol (2,2'-bis-azido-methyl triethylene glycol, called as BAG) in light yellowish was obtained with yield of 88%.

The raw BAG was purified by a Biotage Flash Chromatography (Isolera<sup>™</sup> One, Biotage, USA) using hexanes/ethyl acetate (17%/83% v/v) as mobile phase and silicone gel cartridge as the stationary phase. The desired eluate was collected and rot-evaporated under reduced pressure at 50 °C for 2 h to remove solvent. A transparent liquid BAG monomer was obtained with yield of 74%.

## 2. Synthesis of di-alkyne (DA) crosslinker

The DA crosslinker was synthesized by mixing 5-hexyn-1-ol (2.226 g, 22 mmol) and hexamethylene diisocyanate (HDI) (1.682 g, 10 mmol) in 2 ml dioxane anhydrous (99.0%, ACROS Organics) in a round bottom flask. The reaction was remained at 70 °C for 17 h with magnetic stirring under nitrogen atmosphere. After cool down to room temperature, a white solid product was formed. The raw product was rot-evaporated to remove solvent at 60 °C for 1 h. Then 6 ml tetrahydrofuran (THF, HPLC grade, Alfa Aesar) was added to dissolve the raw product and rot-evaporated to remove the solvent again. The solid was then completely dissolved in 8 ml THF by heating at 60 °C. After cool down to approximately 30 °C, the solution was precipitated in two

50 ml centrifuge tubes filled with 45 ml diethyl ether per tube. The precipitates were settled in a - 20 °C refrigerator overnight and centrifuged to collect the solids. The solvation and precipitation were replicated twice and the solid was further washed twice with diethyl ether to obtain a purified DA product with yield of approximately 78% after drying overnight under reduced pressure at 50 °C.

# 3. Synthesis of azido-functionalized polyurethane

The azido-functionalized polyurethane (APU) was synthesized by condensation polymerization between hexamethylene diisocyanate (HDI), the as-prepared BAG and tetraethylene glycol (TEG). Specifically, HDI (99+%, ACROS ORGANICS) (1.682 g, 10 mmol) and BAG (0.260 g, 1 mmol) were mixed in 2 ml of N,N-dimethylformamide anhydrous (DMF, 99.8%, ACROS ORGANICS). Then 5 µl of di-n-butyltin dilaurate (DBTDL, 95%, Alfa Aesar, dried by molecular sieve) was added as a catalyst to react for 1 h with magnetic stirring under nitrogen atmosphere. Then, TEG (1.748 g, 9 mmol, 99.5%, ACROS ORGANICS, dried by molecular sieve) in 3 ml of DMF were added and the reaction was continued for approximately 20 h under nitrogen atmosphere. The reaction turned to a white gel-like state. The magnetic stirring was discontinued due to the high viscosity. Additional 10 ml DMF was added to dissolve the pre-polymer to yield a clear solution which was then precipitated in two 50 ml centrifuge tubes filled with 40 ml diethyl ether per tube. The solid was collected by centrifugation at 3500 rpm for 15 min. The solvation and precipitation were replicated twice. The solid was then washed twice with diethyl ether and dried under reduced pressure overnight. The solid was further washed with ethanol/deionized water (1:1 v/v) and deionized water under gentle agitation overnight per wash and isolated by centrifugation. The solid was freeze-dried for 48 h to obtain the product with a yield of approximately 87 %.

To examine the reaction efficiency of the BAG monomer with HDI relative to the reaction time, another experiment was conducted by increasing the reaction time of BAG with HDI to 3 h,

followed by adding the TEG segment for further reaction. All other reaction conditions were remained the same. The resultant APU was similarly purified and analyzed by proton NMR analysis to identify the actual azido content.

# 4. Material characterization

The molecular weight of the APU pre-polymer was determined by gel permeation chromatography using Malvern Panalytical OMNISEC GPC system (Malvern Instruments Ltd, UK). The OMNISEC advanced detection system is equipped with triple detectors, including refractive index, right angle and low angle light scattering (RI, RALS and LALS). Advanced detection method was used to determine the molecular weight. Column set of T6000M and T3000 and THF were used as stationary and mobile phases respectively. THF flow rate was set at 1.0 ml/min. The autosampler, column and detector temperatures were set up at 20, 25 and 25 °C respectively. The detection was first calibrated with the company supplied narrow and broad polystyrene standards. The APU pre-polymer was dissolved in HPLC grade DMF at 2.35 mg/ml and filtered through 0.2  $\mu$ m PTFE syringe filter for test. The detection was replicated thrice. M<sub>n</sub>, M<sub>w</sub> and PDI were determined to be 15000  $\pm$  2127 Da, 21930  $\pm$  1230 Da and 1.47  $\pm$  0.12.

The chemical structure and composition of the purified BAG, DA crosslinker and APU prepolymer were characterized by FTIR (NICOLET iS10, Thermo SCIENTIFIC, USA) and ¹H-NMR (400 Hz, Bruker, MA). The purities of the monomer and the crosslinker were examined by HPLC analysis. 10 mg/ml of BAG or DA in methanol was respectively prepared for test using UltiMate 3000 HPLC equipped with UltiMate 3000 variable wavelength detector (ThermoFisher SCIENTIFIC, USA). Methanol and Discovery® C18 column (25 cm x 4.6 mm, 5 μm) were used as mobile and stationary phases. The flow rate of mobile phase was set at 1.000 ml/min with pump pressure at 1107 psi. The detector wavelength was set at 245 nm for detection.

The thermal properties of the APU pre-polymer was examined by DSC analysis (DSC Q200, TA Instrument). 5.67 mg of the APU solid was loaded in an aluminum cuvette and the test

was performed in a heat/cool/heat model under nitrogen atmosphere with flow rate of 50 ml/min. The temperature was first raised from 20 to 450 °C with heating rate at 5 °C/min, followed by cooling down to -80 °C and then raising again to 450 °C. In this way, the change of thermal properties caused by potential chemical reactions could be detected because of the presence of azido groups in the APU pre-polymer.

To further examine the glass transition temperature  $(T_g)$ , melting temperature  $(T_m)$  and crystallization  $(T_c)$  of both the APU pre-polymer and APU elastomer, DSC analysis (MDSC Q1000, TA Instrument) was further performed with the maximal temperature set up at 200 °C without decomposing the polymers. In this case, the heating rate was set at 10 °C/min with the cooling rate at 5 °C/min and nitrogen flow rate at 50 ml/min. 5.6 mg APU pre-polymer and 6.4 mg APU-1.2 elastomer were respectively loaded in a standard Tzero pan with lip. The tests were recorded by first heating up from 25 °C to 200 °C and then cooling down to -60 °C, followed by the second heating up to 200 °C.

# 5. Preparation of APU elastomers

All porous APU elastomers were made by crosslinking APU pre-polymer solutions with DA crosslinker in the presence of copper (I) catalyst at 37 °C for 4 h. First, we prepared a series of APU elastomers with azido to alkyne (Az/Ak) molar ratios ranged from 1.2 to 0.6 for crosslinking while the APU pre-polymer solution at 20 wt./v % was used. These elastomers were made to investigate how the crosslinking density would affect the mechanical properties. Specifically, APU pre-polymer in DMF at 20 wt./v % (~66 mM azido), DA in DMF at 270 mM, CuSO<sub>4</sub> in deionized water at 1 M and Na-L-Ascorbate in DMF/deionized water (1:1, v/v) at 750 mM were prepared for use. To each vial, 1.0 ml of APU solution was respectively mixed with 100, 117, 150 or 200 µl of DA solution. In these mixtures, the Az/Ak molar ratios were 1.2, 1.0, 0.8 and 0.6 respectively for the click reactions. Then, to each vial, 12 µl of CuSO<sub>4</sub> solution was added and mixed by pipetting and gently shaking, followed by quickly mixing with 80 µl of Na-L-Ascorbate solution. The mixture was immediately transferred into a rectangular silicone rubber mode (about 1 mm in thickness)

mounted on a glass slide. All samples were settled in culture dishes with cover and the click reaction was remained in an incubator at 37 °C for 4 h to obtain four APU organogels as the precursors. The organogels were subsequently washed in DMF/10 mM EDTA (1:1 v/v) for 24 h, then 10 mM EDTA, deionized water and 0.9 % saline for 48 h per wash to form APU elastomers. They were named as APU-1.2, APU-1.0, APU-0.8 and APU-0.6 respectively.

To study the effects of pre-polymer concentrations on the mechanical properties, 10, 20 and 30 wt./v % APU in DMF solutions were prepared while the Az/Ak ratio was remained at 1.2 for crosslinking. All other components and procedures were the same as the above. The elastomers were designated as APU-10%, APU-20% and APU-30%.

To study the mechanical properties of a compact APU elastomer with little porous structure, the as-prepared porous APU-1.2 elastomer sheets were freeze-dried and clamped between two glass slides by a medium binder clips (1.25 inch). The samples were fused at 80 °C in an oven for 30 min to form compact APU-1.2 elastomers for mechanical tests. Two catheter materials, poly(vinyl chloride) (PVC) catheter of 16 French (McKesson Medical-Surgical Inc.) and Nylon-12 catheter tube of 11 French (Duke Extrusion) were used to compare the mechanical properties with the compact APU-1.2 elastomer.

# 6. Mechanical property tests

Dog-bone samples were punched from all APU elastomers, PVC catheter and Nylon-12 tube using a dog-bone cutter (3.0x0.5 cm with a neck length of 10.5 mm and width of 1.5 mm). Uniaxial tensile and cyclic tensile (hysteresis) tests were performed according to the standard method (ASTM D412) using Instron 5943 single column testing system equipped with 50N loading cell and Bluehill Universal software (INSTRON®, MA, USA). An elongation rate was set up at 10 mm/min for tensile tests and 30 mm/min for hysteresis tests. The hysteresis tests were repeated thrice to obtain an average cyclic loading numbers for each material; whereas the uniaxial tensile tests for each material were replicated at least four times to obtain the mean value with standard deviation of ultimate tensile strength (UTS), Young's modulus (E) and strain at fracture (%).

# 7. In vitro degradation test

The compact APU-1.2 sheet with thickness of approximately 0.55 mm was cut into rectangular pieces with width of 5 mm and length of 9 mm. The initial mass of each sample was recorded as  $M_0$ . To each sample, 5 ml of 60 mM NaOH solution was added and the degradation test was set in an incubator at 37 °C for 2, 4 and 6 days. At the scheduled time points, the samples were collected, washed completely with deionized water and freeze-dried to record the residual mass as  $M_r$ . The degradation rate was calculated as degradation% =  $(M_0 - M_r) \times 100/M_0$ .

# 8. In vivo biocompatibility study

Male BALB/cJ mice (Jackson Laboratory) with an average age of 8–9 weeks were used and cared for in compliance with a protocol approved by the Institutional Animal Care and Use Committee of the University of Pittsburgh.

The APU elastomeric scaffold prepared in section 5 were punched using a circular puncher with a diameter of 6 mm and thickness of 1 mm. The scaffolds were sterilized by autoclave prior to the subcutaneous implantation. Under isoflurane anesthesia, the APU samples were implanted in the left backs of BALB/cJ mice. At days 3, 28 and 56 after implantation, the animals were sacrificed and the tissues were harvested at the implantation sites. Tissues were fixed in 10% formalin for 15 min, and then soaked in 30% sucrose and embedded in the Tissue-Tek optimum cutting temperature (O.C.T) compound (Sakura Finetek USA). Cross sections (6 µm thick, longitudinal axial cut) were stained with hematoxylin and eosin (H & E), Masson's trichrome stain (MTS) and ED-1 to examine host responses such as inflammation, collagen deposition or any adverse effects. For ED-1 immunohistochemical analysis, the 6 µm thick tissue sections were dried and fixed in histology-grade absolute ethanol for 15 min, air dried, and incubated with rat monoclonal anti-CD68 (1:200, Abcam, Cambridge, MA) for ED-1 identification. The slides were then incubated with a goat anti-rat-Alexa 594 (1:400, Life technologies, Carlsbad, CA) for 1 h. ED-1 stained sections were analyzed for the

population of recruited macrophages. Twelve to twenty-four 200x magnification images were obtained for each specimen. The images were taken using an inverted microscope Eclipse Ti (Nikon, Melville, NY) equipped with a digital camera (Qlmaging, BC, Canada).

To quantify the collagen thickness around the implant, twelve locations from three MTS stained sections per group were selected to measure the collagen thickness to obtain the mean value with a standard deviation. To quantify the CD68 positive macrophages, nine to eighteen immunohistochemically stained sections per group were randomly selected to count the macrophage numbers on each image. The macrophage numbers over each image area (MP number per mm²) were calculated to obtain the mean value with a standard deviation.

# 9. Statistical analysis

Statistical analysis was performed using one-way ANOVA with post-test of Bonferroni or Tukey correction. A p value < 0.05 is considered significant. Data represent the mean  $\pm$  standard deviation (SD).

# **Acknowledgements:**

This work is supported by Cornell Startup Funding. This work made use of the Cornell Center for Materials Research Shared Facilities which are supported through the NSF MRSEC program (DMR-1719875).

#### **Supporting Information.**

Additional data include:

- 1: Proton NMR spectra with the integration analysis
- 2: GPC spectra and molecular weight analysis
- 3: DSC analysis of the APU pre-polymer and the compact APU-1.2 elastomer
- 4: FTIR analysis of the APU-1.2 elastomer to identify unreacted azido groups
- 5: Subcutaneous implantation of APU-1.0 elastomer in mice backs

#### References:

- 1. Guelcher, S. A., Biodegradable polyurethanes: synthesis and applications in regenerative medicine. *Tissue Eng Part B Rev* **2008**, *14* (1), 3-17. DOI: 10.1089/teb.2007.0133.
- 2. Ulery, B. D.; Nair, L. S.; Laurencin, C. T., Biomedical Applications of Biodegradable Polymers. *J Polym Sci B Polym Phys* **2011**, *49* (12), 832-864. DOI: 10.1002/polb.22259.
- 3. Ahmad, S., Polyurethane: A Versatile Scaffold for Biomedical Applications. *Significances of Bioengineering & Biosciences* **2018**, *2* (3). DOI: 10.31031/sbb.2018.02.000536.
- 4. Kutting, M.; Roggenkamp, J.; Urban, U.; Schmitz-Rode, T.; Steinseifer, U., Polyurethane heart valves: past, present and future. *Expert Rev Med Devices* **2011**, *8* (2), 227-33. DOI: 10.1586/erd.10.79.
- 5. Franklin, G.; Harari, H.; Ahsan, S.; Bello, D.; Sterling, D. A.; Nedrelow, J.; Raynaud, S.; Biswas, S.; Liu, Y., Residual Isocyanates in Medical Devices and Products: A Qualitative and Quantitative Assessment. *Environ Health Insights* **2016**, *10*, 175-190. DOI: 10.4137/EHI.S39149.
- 6. Bello, D.; Woskie, S. R.; Streicher, R. P.; Liu, Y.; Stowe, M. H.; Eisen, E. A.; Ellenbecker, M. J.; Sparer, J.; Youngs, F.; Cullen, M. R.; Redlich, C. A., Polyisocyanates in occupational environments: a critical review of exposure limits and metrics. *Am J Ind Med* **2004**, *46* (5), 480-91. DOI: 10.1002/ajim.20076.
- 7. Gabriel, L. P.; Zavaglia, C. A. C.; Jardini, A. L.; Dias, C. G. B. T.; Filho, R. M., Isocyanates as Precursors to Biomedical Polyurethanes. *Chemical Engineering Transactions* **2014**, *38*, 253-258. DOI: 10.3303/CET1438043.
- 8. Choi, J.; Moon, D. S.; Jang, J. U.; Yin, W. B.; Lee, B.; Lee, K. J., Synthesis of highly functionalized thermoplastic polyurethanes and their potential applications. *Polymer* **2017**, *116*, 287-294. DOI: 10.1016/j.polymer.2017.03.083.
- 9. Hahn, C.; Keul, H.; Möller, M., Hydroxyl-functional polyurethanes and polyesters: synthesis, properties and potential biomedical application. *Polymer International* **2012**, *61* (7), 1048-1060. DOI: 10.1002/pi.4242.
- 10. Li, L.; Li, J.; Kulkarni, A.; Liu, S., Polyurethane (PU)-derived photoactive and copper-free clickable surface based on perfluorophenyl azide (PFPA) chemistry. *J. Mater. Chem. B* **2013**, *1* (4), 571-582. DOI: 10.1039/c2tb00248e.
- 11. Choi, J.; Moon, D. S.; Ryu, S. G.; Lee, B.; Lee, K. J., Highly functionalized thermoplastic polyurethane from surface click reactions. *Journal of Applied Polymer Science* **2018**, *135* (29), 46519. DOI: 10.1002/app.46519.
- 12. Fournier, D.; Prez, F. D., "Click" Chemistry as a Promising Tool for Side-Chain Functionalization of Polyurethanes. *Macromolecules* **2008**, *41*, 4622-4630.
- 13. Ito, Y., Covalently immobilized biosignal molecule materials for tissue engineering. *Soft Matter* **2008**, *4* (1), 46-56. DOI: 10.1039/b708359a.
- 14. Grieshaber, S. E.; Farran, A. J.; Bai, S.; Kiick, K. L.; Jia, X., Tuning the properties of elastin mimetic hybrid copolymers via a modular polymerization method. *Biomacromolecules* **2012**, *13* (6), 1774-86. DOI: 10.1021/bm3002705.
- 15. Boffito, M.; Di Meglio, F.; Mozetic, P.; Giannitelli, S. M.; Carmagnola, I.; Castaldo, C.; Nurzynska, D.; Sacco, A. M.; Miraglia, R.; Montagnani, S.; Vitale, N.; Brancaccio, M.; Tarone, G.; Basoli, F.; Rainer, A.; Trombetta, M.; Ciardelli, G.; Chiono, V., Surface functionalization of

polyurethane scaffolds mimicking the myocardial microenvironment to support cardiac primitive cells. *PloS one* **2018**, *13* (7), e0199896. DOI: 10.1371/journal.pone.0199896.

- 16. Xie, Z.; Lu, C.; Chen, X.; Chen, L.; Hu, X.; Shi, Q.; Jing, X., A facile approach to biodegradable poly(ε-caprolactone)-poly(ethylene glycol)-based polyurethanes containing pendant amino groups. *European Polymer Journal* **2007**, *43* (5), 2080-2087. DOI: 10.1016/j.eurpolymj.2007.03.001.
- 17. Marín, R.; de Paz, M. V.; Ittobane, N.; Galbis, J. A.; Muñoz-Guerra, S., Hydroxylated Linear Polyurethanes Derived from Sugar Alditols. *Macromolecular Chemistry and Physics* **2009**, *210* (6), 486-494. DOI: 10.1002/macp.200800517.
- 18. Yang, L.; Wei, J.; Yan, L.; Huang, Y.; Jing, X., Synthesis of OH-group-containing, biodegradable polyurethane and protein fixation on its surface. *Biomacromolecules* **2011**, *12* (6), 2032-8. DOI: 10.1021/bm2003658.
- 19. Ritfeld, G. J.; Rauck, B. M.; Novosat, T. L.; Park, D.; Patel, P.; Roos, R. A.; Wang, Y.; Oudega, M., The effect of a polyurethane-based reverse thermal gel on bone marrow stromal cell transplant survival and spinal cord repair. *Biomaterials* **2014**, *35* (6), 1924-31. DOI: 10.1016/j.biomaterials.2013.11.062.
- 20. Lutz, J. F.; Zarafshani, Z., Efficient construction of therapeutics, bioconjugates, biomaterials and bioactive surfaces using azide-alkyne "click" chemistry. *Adv Drug Deliv Rev* **2008**, *60* (9), 958-70. DOI: 10.1016/j.addr.2008.02.004.
- 21. Riva, R.; Lussis, P.; Lenoir, S.; Jérôme, C.; Jérôme, R.; Lecomte, P., Contribution of "click chemistry" to the synthesis of antimicrobial aliphatic copolyester. *Polymer* **2008**, *49* (8), 2023-2028. DOI: 10.1016/j.polymer.2008.03.008.
- 22. Shibata, Y.; Tanaka, H.; Takasu, A.; Hayashi, Y., Azidation of polyesters having pendent functionalities by using NaN3 or DPPA—DBU and photo-crosslinking of the azidopolyesters. *Polymer Journal* **2011**, *43* (3), 272-278. DOI: 10.1038/pj.2010.135.
- 23. Meng, F.; Qiao, Z.; Yao, Y.; Luo, J., Synthesis of polyurethanes with pendant azide groups attached on the soft segments and the surface modification with mPEG by click chemistry for antifouling applications. *RSC Advances* **2018**, *8* (35), 19642-19650. DOI: 10.1039/c8ra02912a.
- 24. Liu, X.-M.; Thakur, A.; Wang, D., Efficient Synthesis of Linear Multifunctional Poly(ethylene glycol) by Copper(I)-Catalyzed Huisgen 1,3-Dipolar Cycloaddition. *Biomacromolecules* **2007**, *8*, 2653-2658.
- 25. Xu, J.; Prifti, F.; Song, J., A Versatile Monomer for Preparing Well-Defined Functional Polycarbonates and Poly(ester-carbonates). *Macromolecules* **2011**, *44* (8), 2660-2667. DOI: 10.1021/ma200021m.
- 26. Zhang, X.; Zhong, Z.; Zhuo, R., Preparation of Azido Polycarbonates and Their Functionalization via Click Chemistry. *Macromolecules* **2011**, *44* (7), 1755-1759. DOI: 10.1021/ma200137a.
- 27. Guo, J.; Xie, Z.; Tran, R. T.; Xie, D.; Jin, D.; Bai, X.; Yang, J., Click chemistry plays a dual role in biodegradable polymer design. *Adv Mater* **2014**, *26* (12), 1906-11. DOI: 10.1002/adma.201305162.
- 28. Tan, A. C. W.; Polo-Cambronell, B. J.; Provaggi, E.; Ardila-Suarez, C.; Ramirez-Caballero, G. E.; Baldovino-Medrano, V. G.; Kalaskar, D. M., Design and development of low cost polyurethane biopolymer based on castor oil and glycerol for biomedical applications. *Biopolymers* **2018**, *109* (2). DOI: 10.1002/bip.23078.

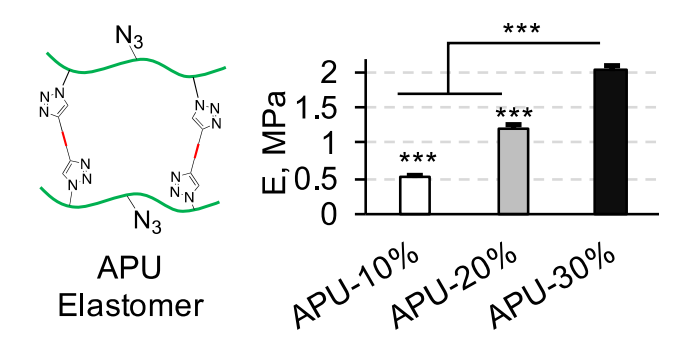
- 29. Pereira, M. J.; Ouyang, B.; Sundback, C. A.; Lang, N.; Friehs, I.; Mureli, S.; Pomerantseva, I.; McFadden, J.; Mochel, M. C.; Mwizerwa, O.; Del Nido, P.; Sarkar, D.; Masiakos, P. T.; Langer, R.; Ferreira, L. S.; Karp, J. M., A highly tunable biocompatible and multifunctional biodegradable elastomer. *Adv Mater* **2013**, *25* (8), 1209-15. DOI: 10.1002/adma.201203824.
- 30. Sabitha, G.; Babu, R. S.; Reddy, M. S. K.; Yadav, J. S., Ring Opening of Epoxides and Aziridines with Sodium Azide using Oxone® in Aqueous Acetonitrile: A Highly Regioselective Azidolysis Reaction. *Synthesis* **2002**, *15*, 2254-2258.
- 31. Buruiana, T.; Melinte, V.; Stroea, L.; Buruiana, E. C., Urethane Dimethacrylates with Carboxylic Groups as Potential Dental Monomers. Synthesis and Properties. *Polymer Journal* **2009**, *41* (11), 978-987. DOI: 10.1295/polymj.PJ2009131.
- 32. Brase, S.; Gil, C.; Knepper, K.; Zimmermann, V., Organic azides: an exploding diversity of a unique class of compounds. *Angewandte Chemie* **2005**, *44* (33), 5188-240. DOI: 10.1002/anie.200400657.
- 33. Pisharath, S.; Ang, H. G., Synthesis and thermal decomposition of GAP–Poly(BAMO) copolymer. *Polymer Degradation and Stability* **2007**, *92* (7), 1365-1377. DOI: 10.1016/j.polymdegradstab.2007.03.016.
- 34. Pourmortazavi, S. M.; Sadri, M.; Rahimi-Nasrabadi, M.; Shamsipur, M.; Jabbarzade, Y.; Khalaki, M. S.; Abdollahi, M.; Shariatinia, Z.; Kohsari, I.; Atifeh, S. M., Thermal decomposition kinetics of electrospun azidodeoxy cellulose nitrate and polyurethane nanofibers. *Journal of Thermal Analysis and Calorimetry* **2014**, *119* (1), 281-290. DOI: 10.1007/s10973-014-4064-0.
- 35. Liang, L.; Astruc, D., The copper(I)-catalyzed alkyne-azide cycloaddition (CuAAC) "click" reaction and its applications. An overview. *Coordination Chemistry Reviews* **2011**, *255* (23-24), 2933-2945. DOI: 10.1016/j.ccr.2011.06.028.
- 36. Chiono, V.; Mozetic, P.; Boffito, M.; Sartori, S.; Gioffredi, E.; Silvestri, A.; Rainer, A.; Giannitelli, S. M.; Trombetta, M.; Nurzynska, D.; Di Meglio, F.; Castaldo, C.; Miraglia, R.; Montagnani, S.; Ciardelli, G., Polyurethane-based scaffolds for myocardial tissue engineering. *Interface Focus* **2014**, *4* (1), 20130045. DOI: 10.1098/rsfs.2013.0045.
- 37. Asadpour, S.; Yeganeh, H.; Ai, J.; Kargozar, S.; Rashtbar, M.; Seifalian, A.; Ghanbari, H., Polyurethane-Polycaprolactone Blend Patches: Scaffold Characterization and Cardiomyoblast Adhesion, Proliferation, and Function. *ACS Biomaterials Science & Engineering* **2018**, *4* (12), 4299-4310. DOI: 10.1021/acsbiomaterials.8b00848.
- 38. D'Amore, A.; Yoshizumi, T.; Luketich, S. K.; Wolf, M. T.; Gu, X.; Cammarata, M.; Hoff, R.; Badylak, S. F.; Wagner, W. R., Bi-layered polyurethane Extracellular matrix cardiac patch improves ischemic ventricular wall remodeling in a rat model. *Biomaterials* **2016**, *107*, 1-14. DOI: 10.1016/j.biomaterials.2016.07.039.
- 39. Ding, X.; Wu, Y. L.; Gao, J.; Wells, A.; Lee, K.; Wang, Y., Tyramine functionalization of poly(glycerol sebacate) increases the elasticity of the polymer. *J Mater Chem B* **2017**, *5* (30), 6097-6109. DOI: 10.1039/C7TB01078H.
- 40. Humphrey, J. D., Continuum biomechanics of soft biological tissues. *Proc. R. Soc. Lond. A* **2003**, *459*, 3-46.
- 41. Zhao, J.; Yu, P.; Dong, S., The Influence of Crosslink Density on the Failure Behavior in Amorphous Polymers by Molecular Dynamics Simulations. *Materials (Basel)* **2016**, *9* (4). DOI: 10.3390/ma9040234.

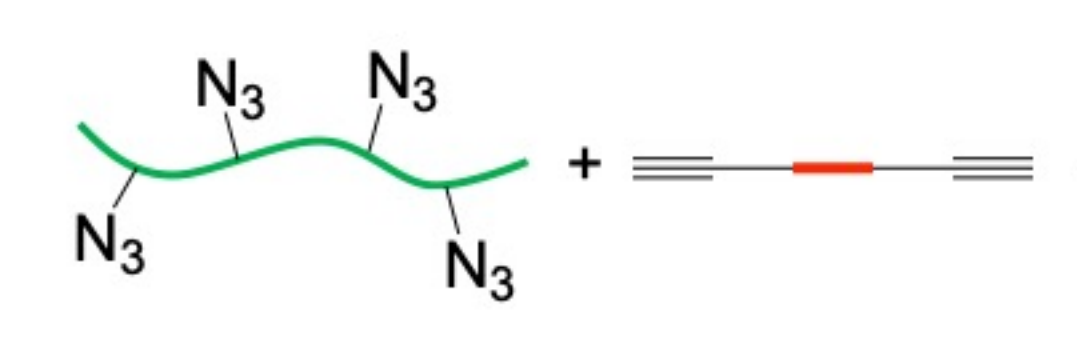
- 42. Maitz, M. F., Applications of synthetic polymers in clinical medicine. *Biosurface and Biotribology* **2015**, *1* (3), 161-176. DOI: 10.1016/j.bsbt.2015.08.002.
- 43. Anderson, J. M., Biological Responses to Materials. *Annu Rev Mater Res* **2001**, *31*, 81-110.
- 44. Ding, X.; Gao, J.; Wang, Z.; Awada, H.; Wang, Y., A shear-thinning hydrogel that extends in vivo bioactivity of FGF2. *Biomaterials* **2016**, *111*, 80-89. DOI: 10.1016/j.biomaterials.2016.09.026.
- 45. Wu, Y.; Sellitti, C.; Anderson, J. M.; Hiltner, A.; Lodoen, G. A.; Payet, C. R., An FTIR-ATR Investigation of In Vivo Poly(ether urethane) Degradation. *Journal of Applied Polymer Science* **1992**, *46*, 201-211.
- 46. McCarthy, S. J.; Meijs, C. F.; Mitchell, N.; Gunatillake, P. A.; Heath, G.; Brandwood, A.; Schindhelm, K., In-vivo degradation of polyurethanes: transmission-FTIR microscopic characterization of polyurethanes sectioned by cryomicrotomy. *Biomaterials* **1997**, *18*, 1387-1409.

# For Table of Contents Use Only

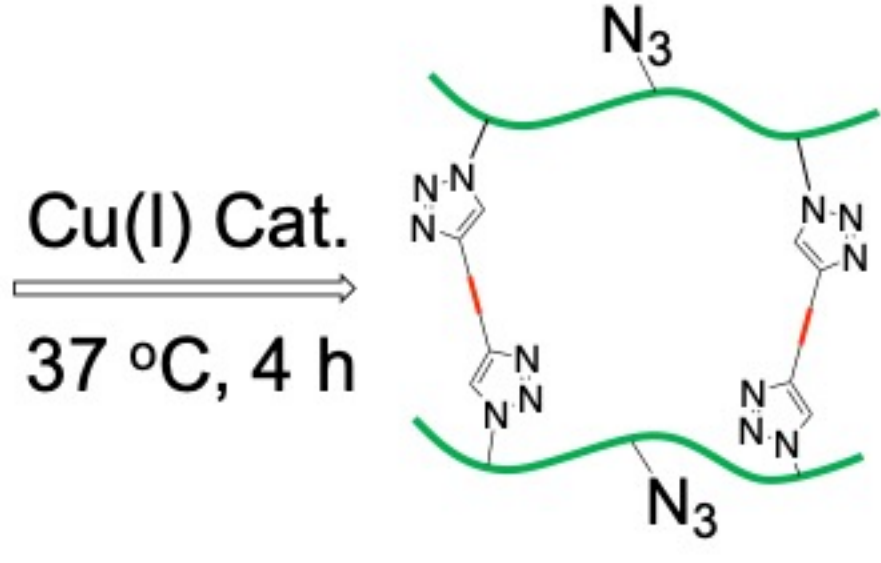
# An azido-functionalized polyurethane designed for making tunable elastomers by click chemistry

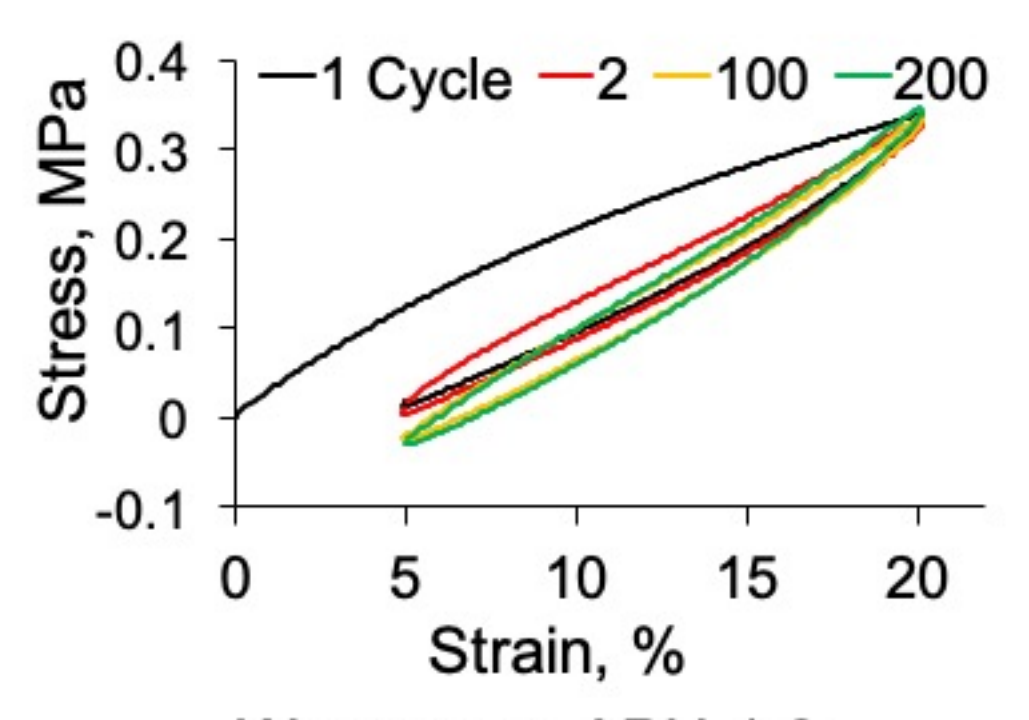
Xiaochu Ding, Jin Gao, Abhinav P. Acharya, Yen-Lin Wu, Steven R. Little and Yadong Wang\*

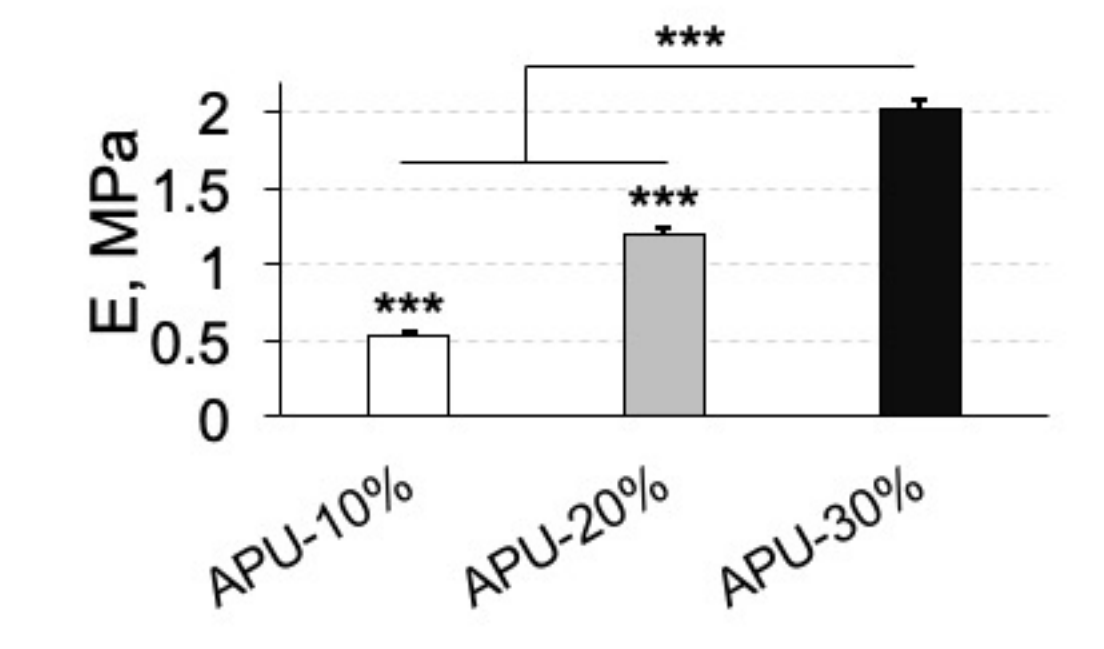




**APU** 







Wet porous APU-1.2 Elastic deformations

Wet porous APU-1.2 Tunable modulus

ACS Paragon Plus Environment